FOCUS REVIEW – Seven Coordinated Molecular Ru-Water Oxidation Catalysts: a Coordination Chemistry Journey

Roc Matheu,[a,b] Mehmed Z. Ertem,[c] Carolina Gimbert-Suriñach,[a] Xavier Sala,[d] and Antoni Llobet[a,d]*

[a] Institute of Chemical Research of Catalonia (ICIQ), Barcelona Institute of Science and Technology (BIST), Avinguda Països Catalans 16, 43007 Tarragona, Spain.

[b] Departament de Química Física i Inorgànica, Universitat Rovira i Virgili, Marcel·lí Domingo s/n, 43007 Tarragona, Spain.

[c] Chemistry Division, Energy & Photon Sciences Directorate, Brookhaven National Laboratory, Upton, New York, 11973-5000, USA

[d] Departament de Química, Universitat Autònoma de Barcelona, Cerdanyola del Vallès, 08193 Barcelona, Spain.

Corresponding author: allobet@iciq.cat

Abstract

Molecular water oxidation catalysis is a field that has experienced an impressive development over the last decade mainly fueled by the promise of generation of sustainable carbon neutral fuel society, based on water splitting. Most of these advancements have been possible thanks to the detailed understanding of the reactions and intermediates involved in the catalytic cycles. Today's best molecular water oxidation catalysts reach turnover frequencies that are orders of magnitude higher than that of natural oxygen evolving center in photosystem II. These catalysts are based on Ru complexes where at some stage, the first coordination sphere of the metal center becomes seven coordinated. The key for this achievement is largely based on the use of adaptative ligands that adjust their coordination mode depending on the structural and electronic demands of the metal center at different oxidation states accessed within the catalytic cycle. This Review covers the latest and most significant developments on Ru complexes that behave as powerful water oxidation catalysts and where at some stage the Ru metal attains coordination number 7. Further it provides a comprehensive and rational understanding of the different structural and electronic factors that govern the behavior of these catalysts.

Keywords.

water oxidation, water splitting, molecular catalysis, redox properties, transition metal complexes, energy conversion.

Table of Contents

1. Introduction.

One of the most diverse families of coordination compounds is the one represented by Ru complexes in part thanks to the large number of formal oxidation states that Ruthenium can access, that range from -2 up to +8.[1] These complexes have a diversified number of applications in many topics including, photochemistry and photophysics,[2,3] bioinorganic chemistry[4,5] and catalysis.[6,7,8,9] From a catalytic point of view, Ruthenium complexes have shown to be active in a significant number of reactions that include, C-H activation and C-C coupling,[7,8] C-H insertion[9] and especially in redox catalysis with organic transformations. [10] The latter includes the oxidation of sulfides to sulfoxides, alkenes to epoxides, alcohols to aldehydes and carboxylic acids. Particularly appealing is the application of Ru derivatives for the catalytic oxidation of water to molecular oxygen as shown in equation 1,[11] since this reaction is fundamental within the context of new renewable and clean[12,13] energy conversion schemes based on water splitting with sunlight.[14,15,16,1718,19]

$O_{2(g)} + 4H^{+}_{(aq)} + 4\ e^{-} \rightarrow 2\ H_2O_{(l)}$ $E^{o} = 1.23$ V *vs*. NHE at pH = 0 (1)

$2\ H^{+}_{(aq)} + 2e^{-} \rightarrow H_{2(g)}$ $E^{o} = 0.0$ V *vs*. NHE at pH = 0 (2)

Indeed, future sustainable energetic schemes rely on technologies that store energy into chemical bonds.[20,21] In this process, also known as artificial photosynthesis, the resulting solar fuels are produced from abundant substrates such as water, carbon dioxide or nitrogen, which are converted to hydrogen, hydrocarbons or ammonia respectively, by means of catalytic reduction reactions.[15,22,23,24] An ideal partner for these reduction reactions is the challenging $4e^{-}/4H^{+}$ oxidation

of H_2O to O_2, that also requires efficient catalysts[25,26,27] and that in combination to the water reduction constitutes the so-called water splitting as shown in equation 3.

$$2\ H_2O_{(l)} \rightarrow O_{2(g)} + 2\ H_{2(g)} \qquad \Delta G^o = 113.5\ \text{kcal/mol} \qquad (3)$$

In this context the water oxidation catalysis field has experienced a significant progress over the last ten years mainly powered by the promise of generation of sustainable carbon neutral fuel, based on water splitting.[28,29,30] Particularly noteworthy has been the development of water oxidation catalysts based on transition metal complexes from the early days of the blue dimer[31] $\{[Ru^{III}(H_2O)(bpy)_2]_2(\mu\text{-}O)\}^{4+}$, **1**, (bpy is 2,2'-bipyridine; see Chart I and Chart II for a drawing of the ligands and complexes respectively that will be discussed throughout this review) in terms of both the performance and the understanding of their reaction mechanisms at a molecular level. For the latter case the main input has been provided by Ru complexes where electrochemical, spectroscopic and reactivity studies together with the detailed characterization of some reaction intermediates and computational modeling has produced a significant degree of knowledge in this topic.[25,32,33,34]

Chart I. Drawing of the ligands discussed in this work.

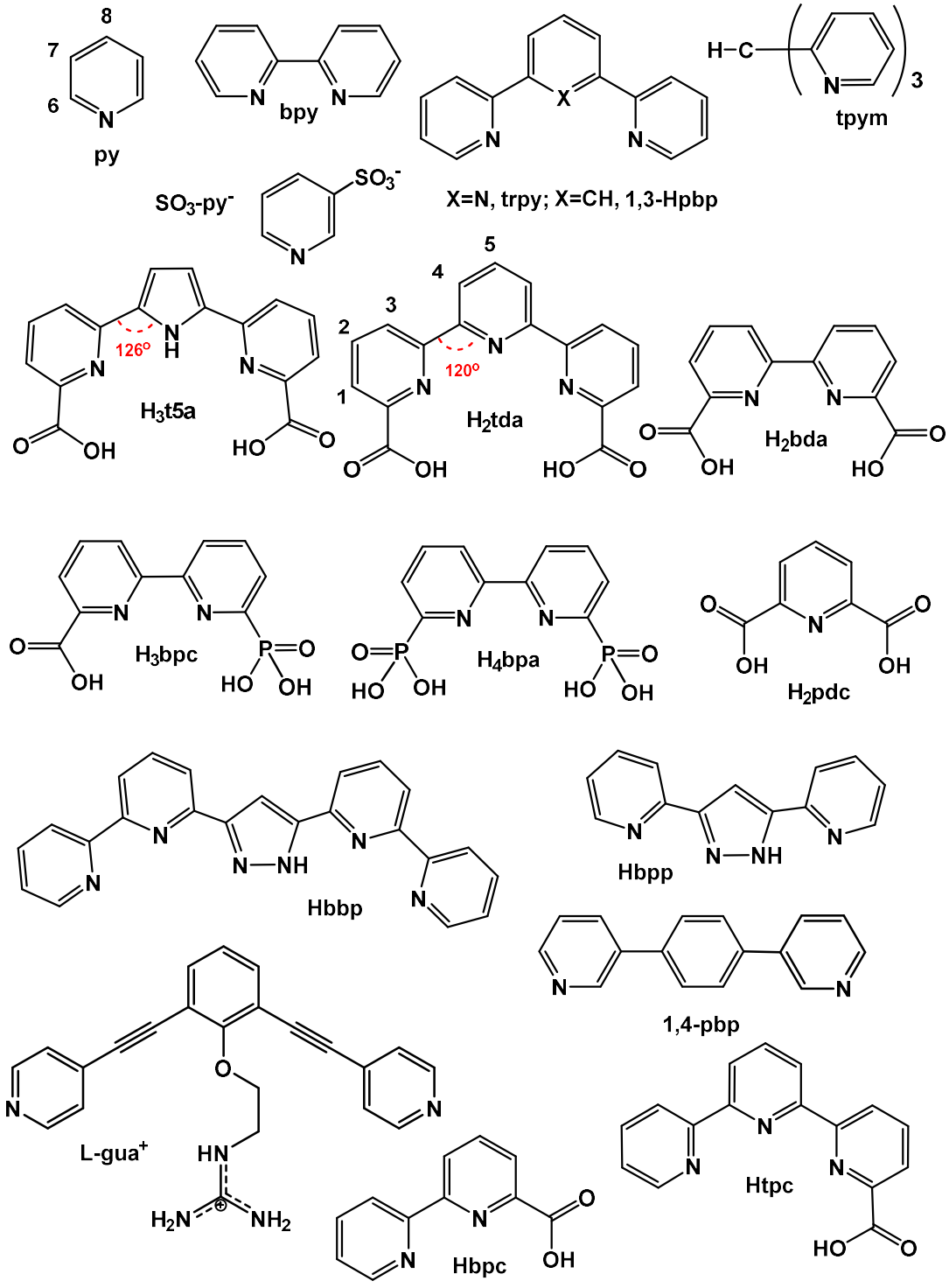

Chart II. Structure drawings of the complexes discussed here.

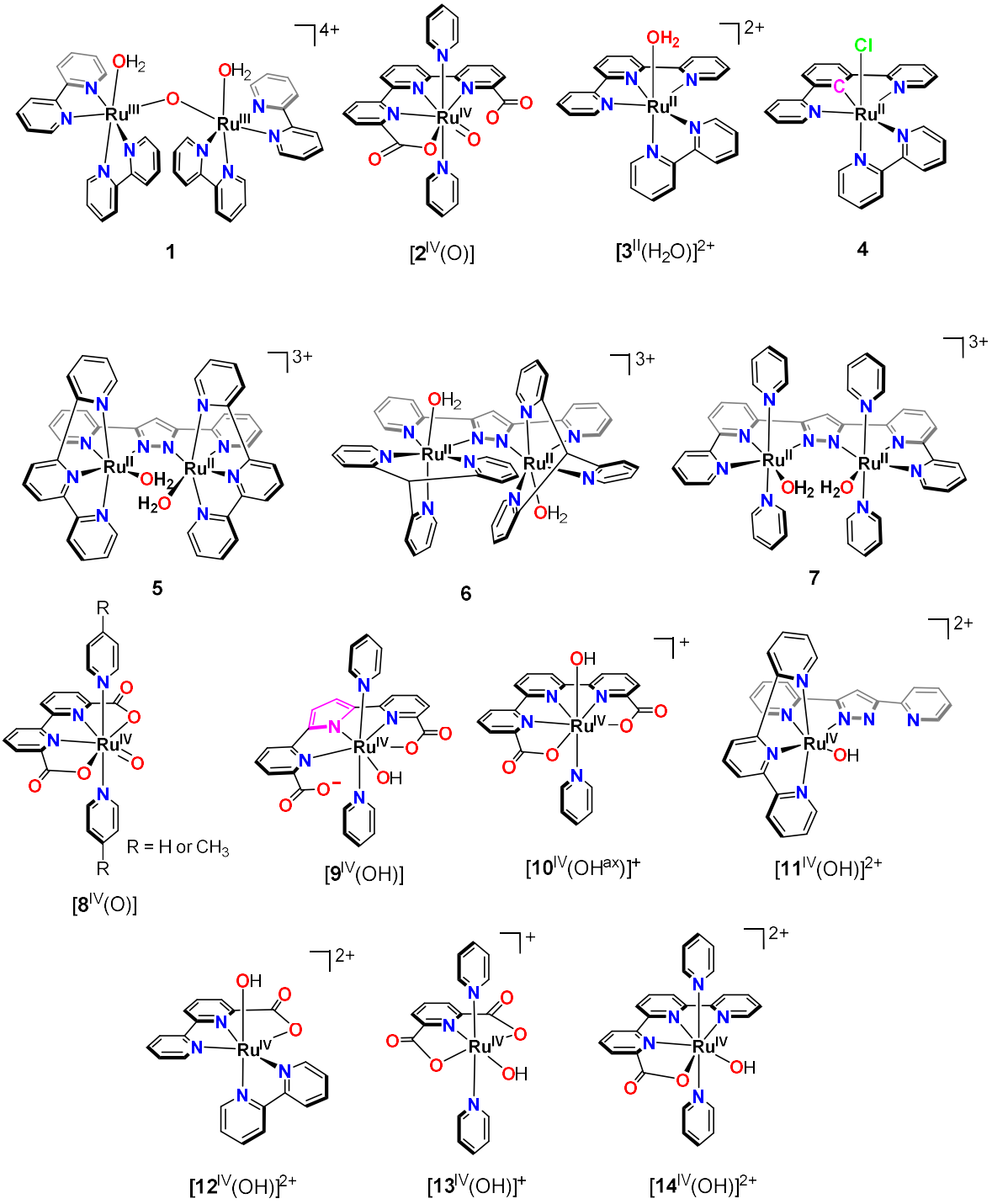

Seven coordinated Ru complexes that contain dianionic ligands such as [2,2'-bipyridine]-6,6'-dicarboxylato (bda^{2-})[35,36] and [2,2':6',2''-terpyridine]-6,6''-dicarboxylato (tda^{2-}) (see Chart I)[37] have given excellent performances based on both efficiency and effectiveness. It is worth mentioning here the impressive performance of the seven coordinated complex $[Ru^{IV}(OH)(tda\text{-}\kappa\text{-}N^3O)(py)_2]^+$, $[\mathbf{2}^{IV}(OH)]^+$, (py is pyridine; See Chart II for a drawing of this complex; $Ru^{IV}(OH)$ -> $Ru^{IV}(O) + H^+$, pK_a = 5.7)[38] that oxidizes water to dioxygen at maximum turnover frequencies (TOF_{MAX}) of 7,700 s^{-1} and 50,000 s^{-1} at pH = 7.0 and pH = 10.0 respectively,[37,39] a value that exceeds 2 orders of magnitude that of Nature's Oxygen Evolving Center at Photosystem II (OEC-PSII) in green plants and algae, that has been reported to turn at the millisecond timescale.[40,41424344] Further for $[\mathbf{2}^{IV}(OH)]^+$ turnover numbers (TONs) higher than one million have been described when anchored into glassy carbon solid electrodes.[45]

Today one of the main goals in the field is to design, develop and incorporate rugged and fast catalysts into unbiased devices for overall water splitting driven by sunlight at neutral to acidic pHs. In order to achieve this challenging goal, it is imperative to further understand the different factors that govern the catalyst's behavior at a molecular level as well as the deactivation and decomposition pathways that operate in parallel, so that they can be circumvented.[46,47,48] Coordination chemistry through molecular transition metal complexes constitutes an excellent ground to examine these factors since significant information based on a large assortment of electrochemical, spectroscopic and analytical techniques can be acquired together with the valuable complementary information provided by theory via computational studies.[49,50,51,52,53,54]

The present focused review is aimed at describing the main features of molecular water oxidation catalysts where at some stage achieve seven coordination around the Ru metal center, and that show an unprecedented performance both in terms of their efficiency and ruggedness.

2. Electronic Structure and Geometrical Features of Ru Complexes.

Today there is a large body of six coordinated Ru complexes reported in the literature where the oxidation state of the metal center is II or III. These RuL_6^{n+} (L is a generic monodentate ligand or monodentate fragment of a polydentate ligand bonded to the metal center) complexes generally possess an octahedral type of geometry, O_h, with a first sphere coordination number of 6 (CN6). In the ideal O_h geometry the angles between the L_{axial}-M-$L_{equatorial}$ (L_{ax}-M-L_{eq}) ligands and L_{eq}-M-L_{eq} ligands are 90° whereas the L_{ax}-M-L_{ax} are 180° as depicted in Figure 1. For O_h type of geometry, the Crystal Field Theory (CFT)[55] predicts a d orbital splitting into a triply degenerate $\boldsymbol{t_{2g}}$ and a doubly degenerate $\boldsymbol{e_g}$ orbitals. Ru complexes at oxidation states IV and above can achieve coordination number of 7 (CN7), generally with a D_{5h} pentagonal bipyramidal coordination geometry.[56,57] In this ideal geometry the angles L_{ax}-M-L_{eq} are still 90° but the L_{eq}-M-L_{eq} angles decrease to 72° as compared to O_h symmetry (see Figure 1). Under D_{5h} geometry the CF splits d orbitals into three sets: two doubly degenerate $\boldsymbol{e_1}''$ (d_{xz}, d_{yz}) and $\boldsymbol{e_2}'$ (d_{xy}, $d_{x^2-y^2}$) orbitals and one $\boldsymbol{a_1}'$ (d_{z^2}) that is higher energy. A plot of these molecular orbitals with significant contribution from the ruthenium 4d atomic orbitals is presented in Figure 2 for the seven coordinated $[Ru^{IV}(tda\text{-}\kappa\text{-}N^3O^2)(py)_2]^{2+}$ complex. Further structural characterization and reactivity of this complex is presented in the following sections.

Octahedral Ru(II) complexes generally have a d^6 high field low spin electronic configuration $(\boldsymbol{t_{2g}})^6(\boldsymbol{e_g})^0$, with paired electrons and thus are diamagnetic. On the other hand, Ru(III) complexes are paramagnetic with d^5 low spin configuration in this geometry, and both configurations are considered substitutionally inert. Further, while Ru(IV) d^4 low spin complexes, $(\boldsymbol{t_{2g}})^4(\boldsymbol{e_g})^0$, with

octahedral geometry are generally paramagnetic, for the corresponding Ru(IV) d^4 low spin CN7 complexes with a D_{5h} geometry are diamagnetic with a $(\boldsymbol{e_1''})^4(\boldsymbol{e_2'})^0(\boldsymbol{a_1'})^0$ electronic configuration.

This is nicely shown in Figure 3 where the ^{1}H NMR spectra of $[Ru^{II}(tda\text{-}\kappa\text{-}N^3O)(py)_2]$, $[Ru^{III}(tda\text{-}k\text{-}N^3O^2)Py_2]^+$ and $[Ru^{IV}(tda\text{-}\kappa\text{-}N^3O^2)(py)_2]^{2+}$ is displayed. For Ru(II) and Ru(IV) the spectra show the typical diamagnetic behavior whereas for Ru(III) it exhibits a paramagnetic shift associated with a complex possessing an electronic configuration with an unpaired electron. On the other hand, while the Ru(II) and Ru(IV) complexes are EPR silent, the Ru(III) complex shows an axial EPR spectrum with $g_{\perp} = 2.0$ and $g_{//} = 2.10$.

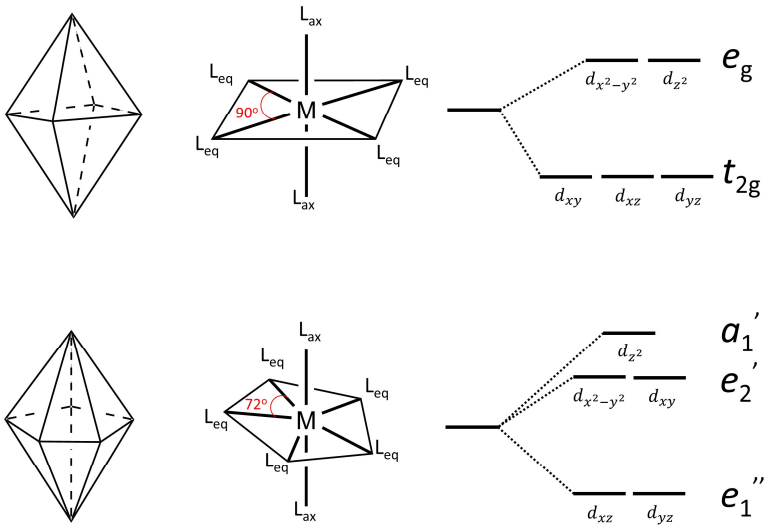

Figure 1. Coordination polyhedra for six (top) and seven (bottom) coordinated transition metal complexes with octahedral (O_h) and pentagonal bipyramidal (D_{5h}) type of geometry. Drawing of the metal-ligand (ML) bonds for the first coordination sphere atoms is presented with Crystal Field Splitting of d-orbitals under these geometries and their corresponding labelling.

Another important property to take into account is the ligand substitution kinetics in ML_6 type of complexes as a function of the nature of the metal center and its electronic structure. For instance, the water exchange rate constants at 298 K for $[Ru^{II}(H_2O)_6]^{2+}$ is $k = 1.8 \times 10^{-2}\ s^{-1}$ and for $[Ru^{III}(H_2O)_6]^{3+}$ is $k = 3.5 \times 10^{-6}\ s^{-1}$.[58] In sharp contrast, the same values for Fe water exchange rate constants are approximately ***eight*** orders of magnitude faster, $k = 4.4 \times 10^{6}\ s^{-1}$ for $[Fe^{II}(H_2O)_6]^{2+}$ and $k = 1.6 \times 10^{2}\ s^{-1}$ for $[Fe^{III}(H_2O)_6]^{3+}$.[59] This is important because water ($[H_2O] = 55.5$ M), will be the solvent in water oxidation catalysis reactions and can seriously compete in the substitution of auxiliary ligands at the first coordination sphere. Progressive substitution of ligands by water will end up with the formation of metal-aquo complexes and free ligand/s in solution. This in turn will favor the activity of the metal as an oxide rather than as a molecular catalyst.

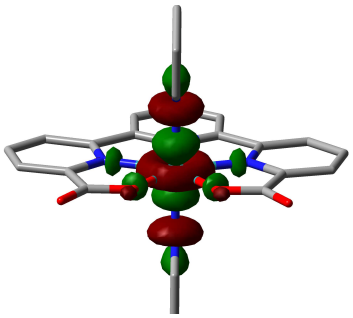

a₁' d_{z^2} (unoccupied)

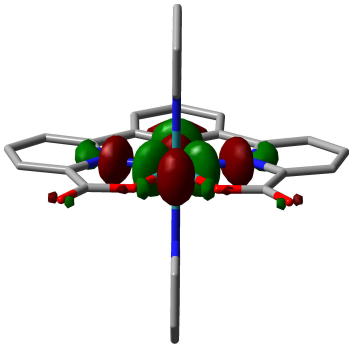

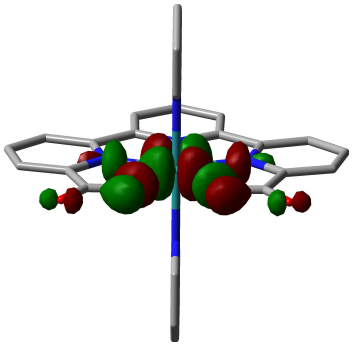

e₂' $d_{x^2-y^2}$ (unoccupied) d_{xy} (unoccupied)

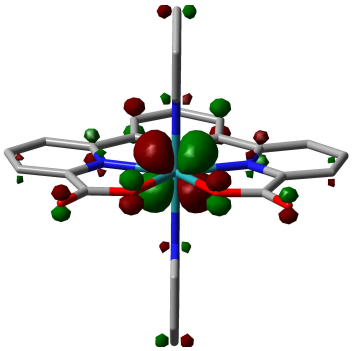

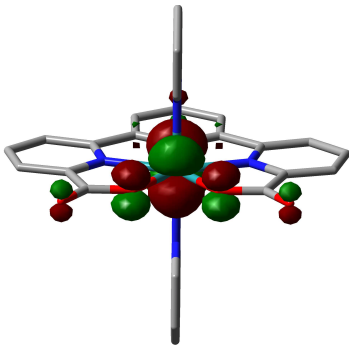

e₁'' d_{xz} (occupied) d_{yz} (occupied)

Figure 2. Plots of molecular orbitals (isofactor = 0.05) with significant contribution from the ruthenium 4d atomic orbitals for seven coordinated $[Ru^{IV}(tda\text{-}\kappa\text{-}N^3O^2)(py)_2]^{2+}$ complex.

.

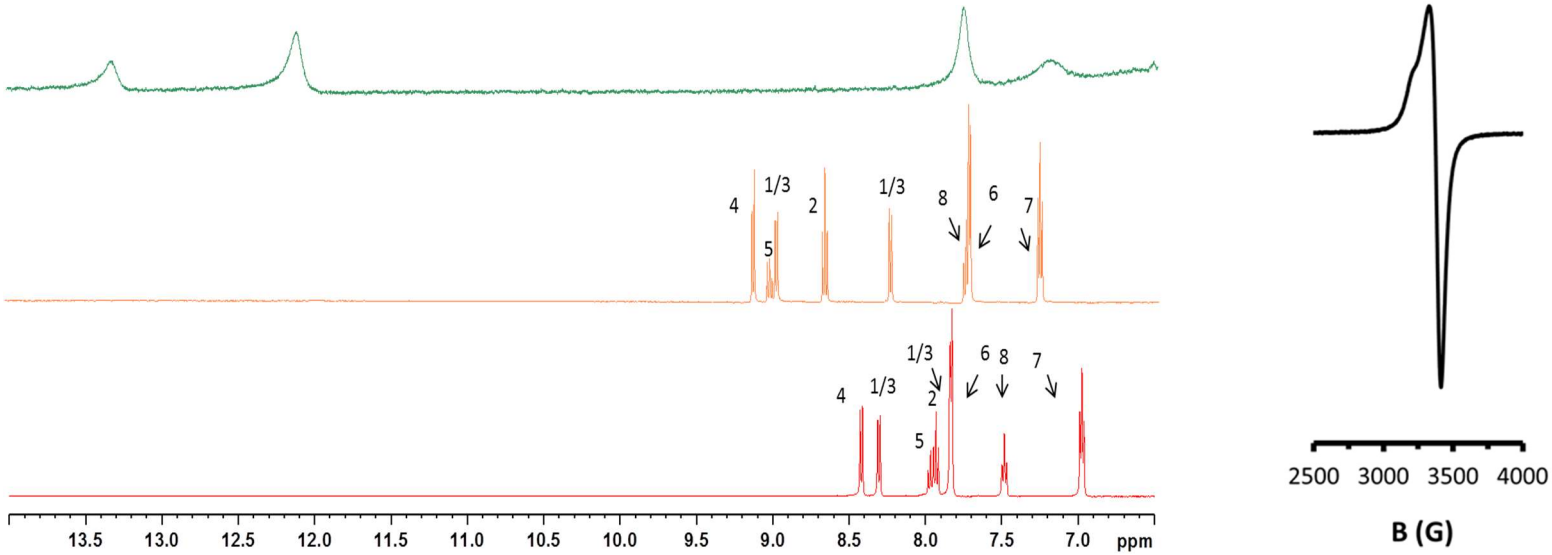

Figure 3. Left, ^{1}H NMR spectra for [Ru^{II}(tda-κ-N^3O)$(py)_2$], (red), [Ru^{III}(tda-κ-N^3O^2)$(py)_2]^+$, (green) and [Ru^{IV}(tda-κ-N^3O^2)$(py)_2]^{2+}$, (orange) in a phosphate buffer pD = 7.0 solution. Right, EPR of [Ru^{III}(tda-κ-N^3O^2)$(py)_2]^+$ at pH = 7.0. The assignment is keyed in Chart I. Reprinted with permission from Reference 37.

3. Ru-aquo High Oxidation States and O-O Bond Formation.

As indicated in equations 1 and 2 the oxidation of water to dioxygen involves the removal of multiple protons and electrons from two water molecules. For this reason, it is highly desirable for a transition metal complex aimed at catalyzing this reaction to be able to access multiple oxidation states. However, when only electrons are removed, a Coulombic charge will be built at the metal center that will produce oxidized species with very high energy that will hinder the subsequent electron removal. On the other hand, the removal of protons and electrons in a concerted fashion, via proton coupled electron transfer (PCET),[60,61,62,63,64] allows access to highly reactive high oxidation states at a relatively low energy cost. An example of this is the $[L_xM\text{-}OH_2]^{n+}$ type of complexes such as $[Ru^{II}(H_2O)(trpy)(bpy)]^{2+}$, $[\mathbf{3}^{II}(H_2O)]^{2+}$, where the electrons are formally removed from the metal center and the protons from the aquo ligand bonded to the transition metal as shown in equation 4.[656667]

$$[L_xM^{II}\text{-}OH_2]^{2+} \underset{+e^-,\,+H^+}{\overset{-e^-,\,-H^+}{\rightleftharpoons}} [L_xM^{III}\text{-}OH]^{2+} \underset{+e^-,\,+H^+}{\overset{-e^-,\,-H^+}{\rightleftharpoons}} [L_xM^{IV}{=}O]^{2+} \qquad (4)$$

A complete description of the dominant species depending on the degree of protonation and protonation can be graphically presented using the corresponding Pourbaix diagram illustrated in Figure 4, that also includes an example of electron removal only complex, $[Ru(Cl)(1,3\text{-}pbp)(bpy)]^{2+}$, **4**, for comparative purposes.[68] The access to different oxidation states within a narrow potential domain is also known as redox leveling and has been described in a number of instances in biology. Particularly relevant is the case for the OEC-PSII where four electrons and four protons are removed as shown in the Kok cycle, depicted in Figure 4.[40,41]

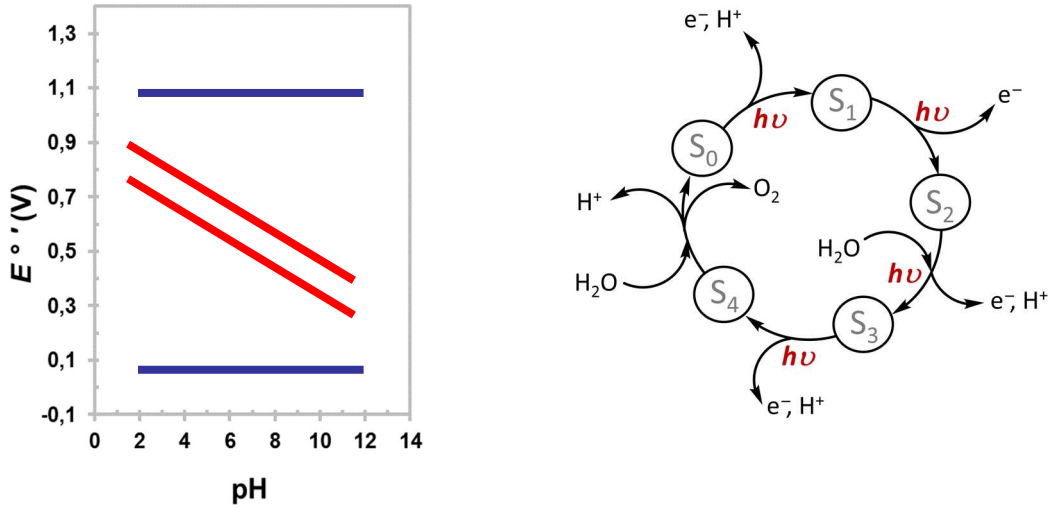

Figure 4. Left, Pourbaix diagram for $[Ru^{II}(H_2O)(trpy)(bpy)]^{2+}$ ($[\mathbf{3}^{II}(H_2O)]^{2+}$, red lines) and $[Ru^{II}(Cl)(1,3\text{-}pbp)(bpy)]^{2+}$ (**4**, blue lines). Right, Kok cycle proposed for the mechanism operating at the tetramanganese Mn_4CaO_5 cluster of the OEC-PSII.

A key feature from an energetic perspective for any $[M\text{-}OH_2]^{n+}$ complex, is the redox potential at which the electron/proton transfers described in equation 4 occur. This is mainly dictated by the metal center, its oxidation state and the coordinating ligands. Because of this, coordination chemistry constitutes an ideal platform for tuning electron density on the metal center and thus redox potentials, through the electronic properties of the ligands. On the other hand, ligand oxidation can be detrimental for the performance of a water oxidation catalyst and therefore the choice of oxidatively rugged ligands is absolutely critical.[69,70,71,72,73] In addition, the fact that some metal oxides (the low energy thermodynamic sink of molecular catalysts), are also catalysts for the water oxidation reaction can generate a profound misinterpretation of the results as has too often been the case in recent years.[74,75,76,77,78]

In equation 4, the of $[L_xM^{IV}=O]^{2+}$ species is generated via removal of $2H^+$ and $2e^-$ from the initial $[L_xM^{II}\text{-}OH_2]^{2+}$ species. This is similar to the removal of $2H^+$ per H_2O molecule indicated in equation 2, which in addition involves the formation of an oxygen-oxygen bond. Thus, the former will be one of the crucial requirements for the design of water oxidation catalysts based on transition metal complexes. On the other hand, from a phenomenological point of view the formation of an O-O bond can take place via the so-called water nucleophilic attack mechanism (WNA) or by interaction of two M-O units (I2M) as presented in Figure 5, for the dinuclear complexes $\{[Ru^{II}(H_2O)(trpy)]_2(\mu\text{-bpp})\}^{3+}$, **5**,[79,49] $\{[Ru^{II}(H_2O)(tpym)]_2(\mu\text{-bpp})\}^{3+}$, **6**,[80] and $\{[Ru^{II}(H_2O)(py)_2]_2(\mu\text{-bbp})\}^{3+}$, **7**.[81] For dinuclear di-aquo complexes the I2M mechanism can potentially occur via both intra- or inter- molecular manner as it happens in **5** and **6** respectively or via WNA as is the case of **7**. The same mechanisms apply for mononuclear ruthenium complexes that have shown to operate via WNA[37] or I2M[35] depending on the nature of the catalyst and reaction conditions.

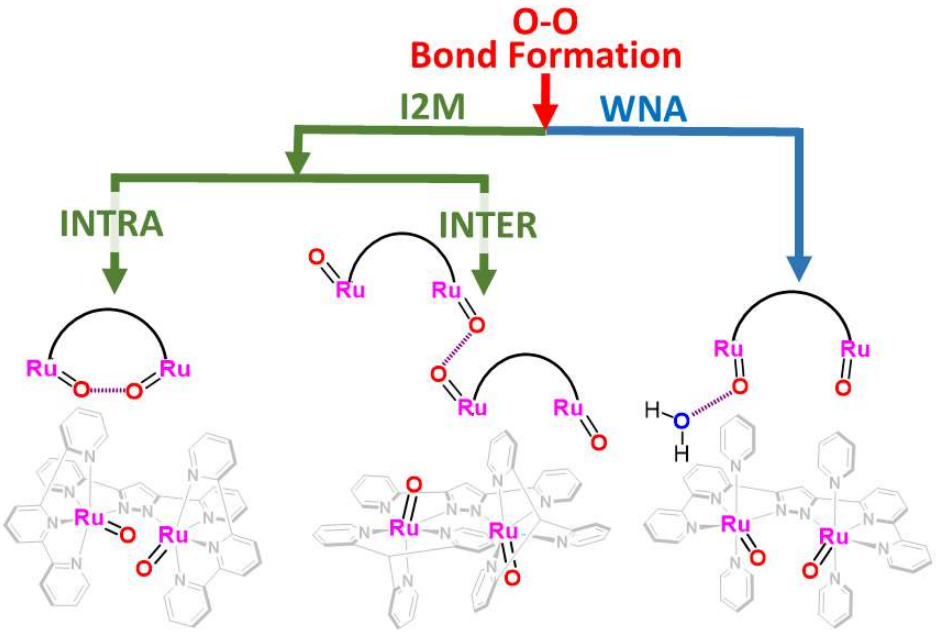

Figure 5. O-O bond formation pathways for the water oxidation reaction exemplified for selected dinuclear Ru complexes (**5**, left; **6**, center; **7**, right). The black arc represents the bridging ligands.

4. Ligand Influence on the Geometrical and Dynamic Properties of Ru Water Oxidation Catalysts: Isomerism, Fractional Coordination and Multiple Equilibria.

Among the fastest ruthenium water oxidation catalysts reported so far are the $[Ru^{IV}(OH)(tda\text{-}\kappa\text{-}N^3O)(py)_2]^+$, $[\mathbf{2}^{IV}(OH)]^+$ and $[Ru^{IV}(OH)(bda\text{-}\kappa\text{-}N^2O^2)(Me\text{-}py)_2]$, $[\mathbf{8}^{IV}(OH)]^+$, complexes containing penta- and tetradentate ligands respectively where the tda^{2-} and bda^{2-} ligands occupy the equatorial position of the first coordination sphere of the Ru center (see Chart I and II). The axial positions are completed with monodentate pyridyl type of ligands such as pyridine (py) or 4-methylpyridine (Me-py). In both cases the initial complexes at low Ru(II) oxidation state do not contain the indispensable Ru-aquo site for the O-O bond formation and thus are not catalysts but catalyst precursors. The required aquo ligands coordinate to Ru when the complex is dissolved in water or upon reaching higher oxidation states. These two families of Ru-complexes achieve CN7 at high oxidation states but their mode of action is significantly different and their coordination geometry changes as a function of their formal oxidation state.

The $[Ru^{II}(tda\text{-}\kappa\text{-}N^3O)(py)_2]$, $[\mathbf{2}^{II}(\kappa\text{-}N^3O)]$,[82] constitutes an excellent ground to grasp the complexity and richness of the coordination geometry of the metal center as a function of oxidation state and solvent and thus will be presented as a model. An ORTEP plot of the crystal structure of complex $[\mathbf{2}^{II}(\kappa\text{-}N^3O)]$ is displayed in Figure 6, top. For $[\mathbf{2}^{II}(\kappa\text{-}N^3O)]$, the tda^{2-} coordinates at the equatorial plane in a $\kappa\text{-}N^3O$ fashion where one of the carboxylato ligands is dangling and non-coordinated. The axial positions are completed by the pyridyl ligands. The geometry of the equatorial plane is highly distorted due to the geometrical constrains imposed by the tda^{2-} ligand; this is exemplified by the $L_{eq}\text{-}M\text{-}L_{eq}$ angles displayed in the lower part of Figure 6. As can be observed the tda^{2-} forces a NRuO angle of 125° in contrast to the ideal 90° degrees of a typical octahedral coordination. When a monodentate ligand such as water replaces the bonded carboxylate in $[\mathbf{2}^{II}\text{-}\kappa\text{-}N^3O]$,

generating [$Ru^{II}(H_2O)$(tda-κ-N^3)$(py)_2$], [**2**$^{II}(H_2O)$(κ-N^3)], it releases the tda^{2-} ligand constraint and now the equatorial angles are within the range of 80-100° (see Figure 6, bottom), closer to the ideal 90°.[83,84]

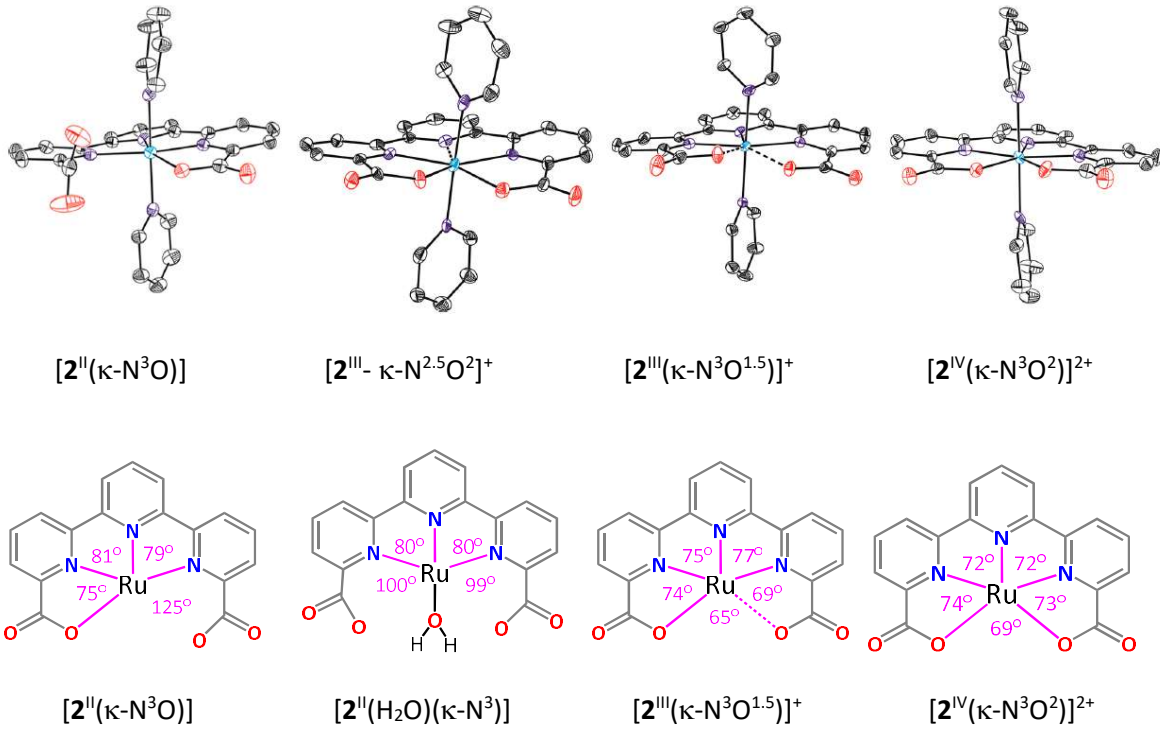

Figure 6. Top, ORTEP drawings of Ru-tda complexes **2** at oxidation states II, III and IV. Bottom, bond angles for the equatorial ligands extracted from the corresponding X-ray structures. Axial ligands not shown for clarity. Broken lines represent contacts. The crystal structure of [**2**$^{II}(H_2O)$(κ-N^3)] is not shown in the upper part. The data is extracted from reference 84.

The large NRuO angle in [**2**^{II}(κ-N^3O)], and the presence of the dangling carboxylate are responsible for a fast dynamic behavior observed in non-coordinating solvents at room temperature. This has been evidenced by NMR spectroscopy where at room temperature the resonances of the tda^{2-} ligands appear as if the ligand had C_{2v} symmetry due to the interconversion of the pyridyl carboxylate arms bonded to the central pyridyl group. At a sufficiently low temperature the

equilibrium slows down and thus splits the resonances of the two arms. This is depicted in cycle A at the left hand side of Figure 7.

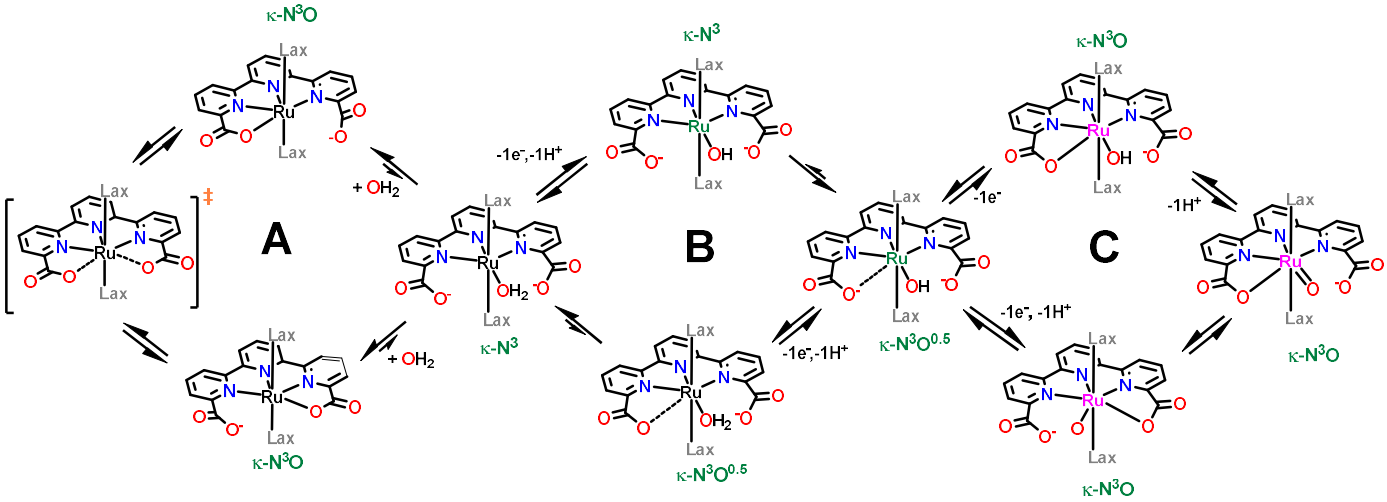

Figure 7. Multiple equilibria for Ru-tda complexes **2** at oxidation states II-IV (color labeling: black = Ru(II); green = Ru(III); magenta = Ru(IV)).

The one electron oxidation of $[Ru^{II}(tda\text{-}\kappa\text{-}N^3O)(py)_2]$, $[\mathbf{2}^{II}(\kappa\text{-}N^3O)]$, generates $[\mathbf{2}^{III}]^+$ where now the Ru metal center has oxidation state III and whose ORTEP plot is shown in Figure 6. The crystal structure contains two different linkage isomers in the unit cell where tda^{2-} ligand is bonded in a $\kappa\text{-}N^3O^{1.5}$ and $\kappa\text{-}N^{2.5}O^2$ modes $[\mathbf{2}^{III}(\kappa\text{-}N^3O^{1.5})]^+$, $[\mathbf{2}^{III}\text{-}\kappa\text{-}N^{2.5}O^2]^+$ respectively.[85] The fractional coordination number is used to denote the presence of a contact, with Ru-N or Ru-O distances in the range of 2.4-2.7 Å. We will refer to this contact as a half coordination and thus the coordination number for these complexes at oxidation state III is 6.5. In solution the two isomers interconvert rapidly as evidenced by a single transition in the EPR spectrum and by the low energy of activation obtained for their interconversion based on density functional theory (DFT) calculations. This equilibrium between the two isomers looks as if the metal center is travelling within the two sides of the tda^{2-} ligand framework resembling a metal oscillator movement.

Further one electron oxidation of $[\mathbf{2}^{III}]^{+}$, generates $[\mathbf{2}^{IV}(\kappa\text{-}N^3O^2)]^{2+}$, $[\mathbf{2}^{IV}]^{2+}$, where the Ruthenium metal center has oxidation state IV. Its crystal structure is presented in Figure 6, and shows that now the tda^{2-} ligand coordinates in a $\kappa\text{-}N^3O^2$ manner occupying the five equatorial positions of a pentagonal bipyramid. Two pyridine ligands occupy the axial positions completing a D_{5h} type of geometry. The $L_{eq}\text{-}M\text{-}L_{eq}$ angles in the equatorial zone are in the range of 69-74° (see Figure 6, bottom), very close to the 72° expected for an ideal D_{5h} geometry, thus clearly demonstrating the capacity of the tda^{2-} ligand to favor this geometrical arrangement. Within this crystal field the Ru(IV) metal center has a low spin d^4 $(\boldsymbol{e_1''})^4(\boldsymbol{e_2'})^0(\boldsymbol{a_1'})^0$ electronic configuration and is diamagnetic at room temperature. The NMR spectrum of the $[\mathbf{2}^{IV}]^{2+}$ complex is highly symmetric and a bit shifted to low fields as compared to that of $[\mathbf{2}^{II}]$ as can be observed in Figure 3. This confirms that the solid state geometry is maintained in solution.

When dissolved in water complex $[\mathbf{2}^{II}]$ is in equilibrium with the aquo complexes $[\mathbf{2}^{II}(H_2O)(\kappa\text{-}N^3)]$ and $[\mathbf{2}^{II}(H_2O)(\kappa\text{-}N^3O)]$, as shown in the A-square cycle in Figure 7, where the equilibrium is highly shifted toward the non-aquated complex. At pH 7, one electron oxidation generates $[\mathbf{2}^{III}(OH)(\kappa\text{-}N^3)]$ that rearranges quickly to the CN6.5 complex $[\mathbf{2}^{III}(OH)(\kappa\text{-}N^3O^{0.5})]$, as shown in the B cycle of Figure 7, that is also in equilibrium with the non-aquated species (not shown in the figure), as deduced from electrochemical experiments and theoretical calculations. Further one electron oxidation leads to seven coordinated $[\mathbf{2}^{IV}(OH)(\kappa\text{-}N^3O)]^{+}$ complex, where one of the carboxylate moieties of the tda^{2-} is not coordinated.

Theoretical calculations indicated the easy formation and breaking of a Ru-O-carboxylate bond. It thus suggests the existence of a dynamic behavior underlined in the Square C of Figure 7, even at room temperature. This once again manifests the flexibility of the tda^{2-} ligand even at oxidation state IV.

The different coordination modes displayed by the tda^{2-} at the different oxidation states of the metal center is a good example of an adaptative ligand capable to accommodate to the structural and electronic demands of the different intermediates accessed within a catalytic redox cycle.

Another interesting system that is worth mentioning here is the one constituted by the family of Ru complexes containing the trianionic $t5a^{3-}$ ligand including $[Ru^{IV}(t5a\text{-}\kappa\text{-}(N^3O^2)py_2)]^+$, $[\mathbf{9}^{IV}]^+$, see Chart I and II. Here the central pyridyl ring of tda^{2-} is replaced by a five-member pyrrole ring, whose NH proton is relatively acidic and which thus coordinates to the metal center as a pyrrolide. This has tremendous consequences for the coordination properties of the metal center both from an electronic but also from a structural perspective even though the $t5a^{3-}$ ligand is still pentadentate.[86]

From a structural point of view, the replacement of six- by a five-membered ring in the ligand framework increases the CCN angles from 120° to 126° as shown in Chart I (in red), and thus further constrains the coordination around the Ru center. This, added to the large electron density delivered by the pyrrolide moiety generates a pseudo-octahedral Ru(II) complex with a rare CN5.5 as predicted by DFT calculations for $[Ru^{II}(t5a\text{-}\kappa\text{-}N^{2.5}O)(py)_2]^-$, $[\mathbf{9}^{II}(\kappa\text{-}N^{2.5}O)]^-$ (see Figure 8, left). The fractional coordination value here corresponds to the Ru-N distance of 2.5 Å shown with a dashed line in the Figure.

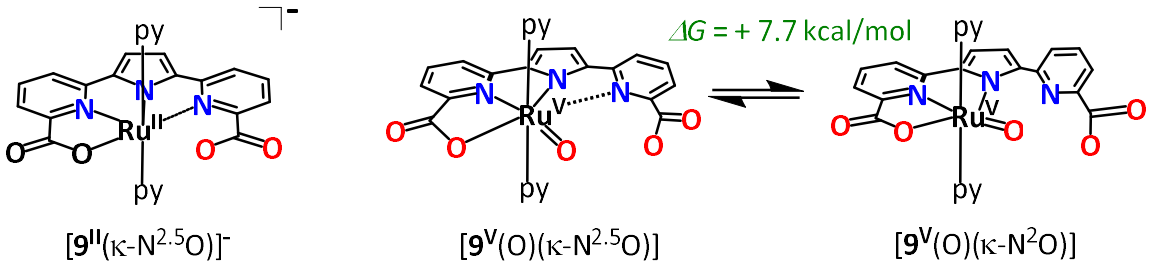

Figure 8. Left, drawn structure of complex $[Ru^{II}(t5a\text{-}\kappa\text{-}N^{2.5}O)(py)_2]^-$, $[\mathbf{9}^{II}(\kappa\text{-}N^{2.5}O)]^-$. Right, drawing of DFT optimized structures for $[\mathbf{9}^{V}(O)]$ isomers and their relative free energies.

Also, it is interesting to note that at high oxidation states, the additional constraints imposed by the 12° angle decrease due to the $t5a^{3-}$ ligand structure, together with the additional electron density supplied by the two anionic donor atoms of this ligand, give rise to two Ru(V) complexes namely, $[Ru^{V}(O)(t5a\text{-}\kappa\text{-}N^{2.5}O)(py)_2]$, $[\mathbf{9}^{V}(O)(\kappa\text{-}N^{2.5}O)]$ and $[Ru^{V}(O)(t5a\text{-}\kappa\text{-}N^{2}O)(py)_2]$, $[\mathbf{9}^{V}(O)(\kappa\text{-}N^{2}O)]$, with 6.5 and 6 coordination number which are close in energy as evidenced by DFT calculations (see Figure 8 right). Thus, the combination of additional geometrical distortion and increased electron donation from the ligand results in the destabilization of seven-coordination, CN7, at high oxidation states.

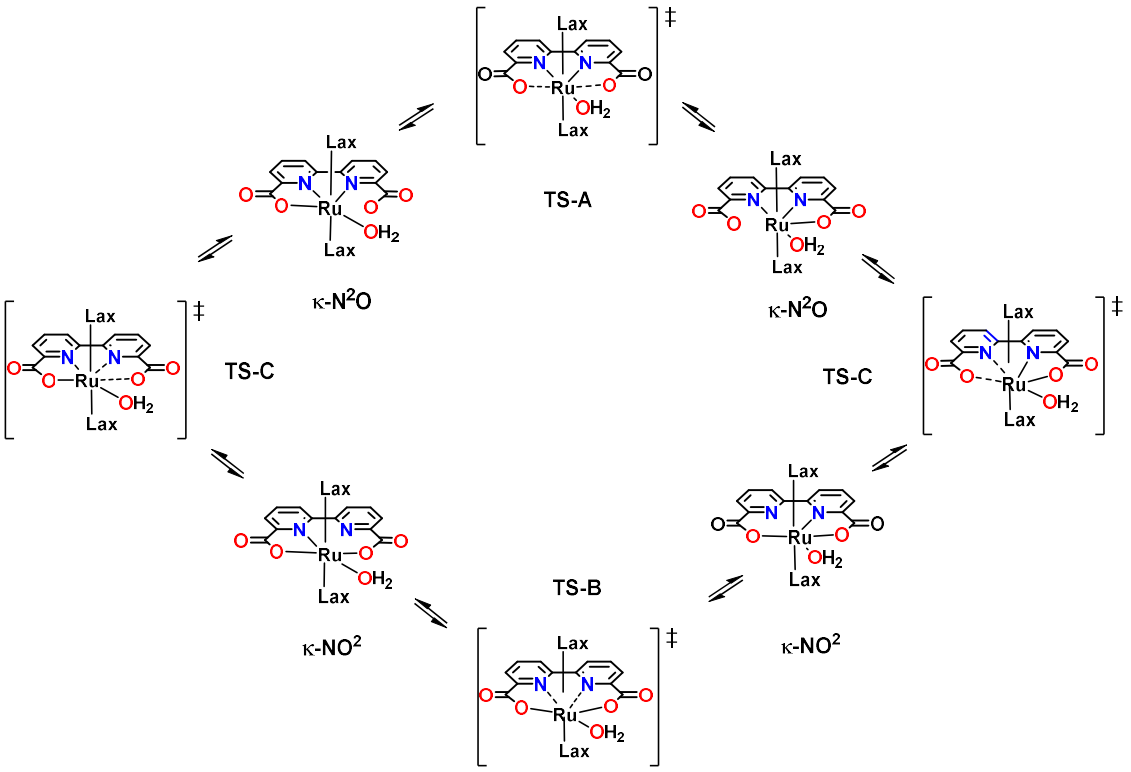

Figure 9. Multiple equilibria associated with the dynamic behavior of aquated Ru complex **8** at oxidation state II. The κ notations refer to the mode of coordination of the bda^{2-} ligand at each structure. L_{ax} represents the axial ligand, usually pyridine.

Finally, another interesting ligand that also shows a good degree of flexibility is the bda^{2-} (see Chart I). At oxidation state II the $[Ru^{II}(bda\text{-}\kappa\text{-}N^2O^2)(py)_2]$, $\mathbf{8}^{II}$, complex in the absence of a coordinating solvent has a distorted O_h geometry similar to that of the Ru-tda, $[\mathbf{2}^{II}(\kappa\text{-}N^3O)]$ discussed above, but without the dangling carboxylate. However, in the presence of coordinating ligands such as H_2O, NO^+ or MeCN the scenario changes radically. In water, at pH = 1 a dynamic behavior is observed where a series of equilibria occur as shown in Figure 9, which involves the coordination of a solvent water molecule to the metal center to form $[Ru^{II}(H_2O)(bda\text{-}\kappa\text{-}N^2O)(py)_2]$, $[\mathbf{8}^{II}(H_2O)(\kappa\text{-}N^2O)]$, and $[Ru^{II}(H_2O)(bda\text{-}\kappa\text{-}NO^2)(py)_2]$, $[\mathbf{8}^{II}(H_2O)(\kappa\text{-}NO^2)]$, with concerted formation and

breaking of both Ru-N and Ru-O bonds.[87] This dynamic behavior has been established for the Ru-bda complex both at oxidation state II and III based on NMR, XAS, electrochemistry and complemented with DFT calculations. Interestingly, here the relative stability of species [**8**^{II}(H_2O)(κ-NO^2)], where one of the bda^{2-} pyridyl N-atom is decoordinated, is assisted by substantial H-bonding with the coordinated carboxylate moieties of the ligand and the Ru-OH_2 group forming a second coordination sphere belt. Thus supramolecular second coordination sphere effect is responsible for the very unusual κ-NO^2 coordination mode at low oxidation states. At oxidation state IV the Ru metal center generates a CN7, D_{5h} complex where the coordinated aquo ligand loses a proton and generates [Ru^{IV}(OH)(bda-κ-N^2O^2)(Me-py)$_2$]$^+$, [**8**^{IV}(OH)]$^+$.[88] Variation of this Ru complex with the replacement of one or two of the carboxylate moieties of the H_2bda ligand by phosphonate groups to form H_3bpc and H_4bpa respectively (see Chart I) has also been reported recently.[89,90,91] These new complexes display different behavior from the parent complex [**8**^{IV}(OH)]$^+$ due to the structural changes caused by the tetrahedral geometry of the phosphonate group and to the additional proton content. Their main impact on the catalytic behavior towards the water oxidation reaction is discussed in section 6.

5. Ligand Influence on Thermodynamics: E^o and pK_a.

As shown in the previous section, Ru-aquo complexes containing polypyridyl ligands like [Ru^{II}(H_2O)(trpy)(bpy)]$^{2+}$, [**3**^{II}(H_2O)]$^{2+}$, can exhibit a number of electron transfer and/or PCET events that lead to the formation of Ru species at high oxidation states. The latter are then capable of promoting O-O bond formation, which after several steps leads to the formation of dioxygen. In the majority of the cases described in the literature, this occurs by reaching the Ru(V) formal oxidation state and thus the redox potential of the Ru^V=O/Ru^{IV}=O couple, or the corresponding Ru^{IV}-OH

species depending on the pH, is crucial and basically determines the overpotential at which the electrocatalysis occurs.[32,35,36,37,46] It is thus essential to understand how ligands can potentially affect the redox potential of this couple and achieve water oxidation catalysis at a redox potential close to the thermodynamic value of the $4H^+/4e^-$ low energy path.

There are mainly two different ways the ligands can perturb the electron density at the ruthenium center: directly or in a remote manner. The direct perturbation involves neutral and/or anionic ligands with different atoms bonding to the metal center at its first coordination sphere. On the other hand, a remote electronic perturbation can be achieved by using electron donating or withdrawing substituents at the backbone for instance of a pyridyl ligand. The latter approach has been developed in a number of cases,[92,93,94,95] but the results obtained in terms of reducing overpotentials and increasing TOFs are generally poor due to the small effect exerted to the Ru(V)/Ru(IV) couple.

Table 1: Structural, thermodynamic and kinetic properties of selected Ru-aquo complexes.

Complex	**10**^{IV}(OH^{ax})$^{+}$	**8**^{IV}(OH)$^{+}$	**2**^{IV}(OH)$^{+}$	**14**^{IV}(OH)$^{2+}$	**9**^{IV}(O)$^{-}$	**13**^{IV}(O)	**12**^{IV}(O)$^{+}$	**11**^{IV}(O)$^{+}$	**3**^{IV}(O)$^{2+}$
Ru^{IV}-OH Coord. Environment[a]	4py, 2COO^{-}	4py, 2COO^{-}	5py, 1COO^{-}	5py, 1COO^{-}	3py, 1COO, 1pyrrolid	3py, 2COO^{-}	4py, 1COO^{-}	4py, 1pyr^{-}	5py
Coord. Number (n^{-})	7 (2)	7 (2)	7 (1)	7 (1)	6 (2)	6 (2)	6 (1)	6 (1)	6 (0)
p*K$_{a;}$ Ru^{IV}-OH/Ru^{IV}-O*	13.5	6.0	5.7	n.a.[c]	7.4	n.a.[c]	< 1.0	< 1.0	<1.0
(Calc.)[b]	(11.8)	(6.8)	(5.4)			(2.9)	(-2.6)	(-7.7)	(-8.9)
E^{o} Ru^{V}=O/Ru^{IV}=O (V)	1.12	1.12	1.43	1.40	1.43	1.35	1.59	1.59	1.86
(Calc.)[b]	(0.97)	(1.04)	(1.26)			(0.95)	(1.33)	(1.60)	(1.76)
η (V) at *pH 7*[d]	0.68	0.30	0.61	n.a.[c]	0.67	0.53	0.77	0.77	1.04
BDE (Kcal/mol)[e]	-117.9	-107.6	-114.4	- -	-116.8	-108.7	-106.8	-99.8	-104.4
TOF$_{max}$ at pH 7 (s^{-1})	0.4[f]	25[g]	7,700[f]	--	9,400[f]	--	--	1.0[g]	0.05[g]
Reference	83	35+39	37 + 39	100	86	99	98	97	93

[a]In this row, py represents the monodentate pyridyl ligand or a pyridyl group of an auxiliary ligand while COO^{-} represents the carboxylato group of the corresponding ligand. The abbreviation pyr^{-} is for the anionic pyrazolato group. [b]Calculated based on DFT. [c]n.a. means not available. [d]Calculated as *E^{o} (Ru^{V}=O/Ru^{IV}=O) - E^{o} (O$_2$/H$_2$O)* in V at pH = 7. [e]BDE, homolytic bond dissociation energies for Ru^{IV}O-H in kcal/mol, calculated using the Bordwell[101] equation. [f] Calculated using foot of the wave analysis, FOWA,. at pH = 7.0 (phosphate buffer, 43 mM) following the procedure described in reference 39, [g] TOF = 25 s^{-1} measured manometrically; TOF$_{max}$ = 11 s^{-1} measured electrochemically using FOWA.

In sharp contrast, changing the first coordination sphere atoms with strong sigma-donor ligands has proven to be a very successful approach, especially using carboxylate and phosphonate moieties.[92,96] For this purpose, several ligands containing a combination of pyridyl and carboxylate (or phosphonate) groups have been designed (See Chart I), which when coordinated to the metal center can act in a mono-, di- or trianionic manner and thus will be strongly influencing the redox properties of the corresponding complexes. Further, the amount of electron density supplied from the ligands to the metal center will also be influenced by the coordination number and mode of the latter. Several Ru-aquo complexes (**2**, **3**, **8**, **9**, **10, 11, 12, 13, 14**), containing the above mentioned ligands have been reported with a detailed description of their redox properties that are summarized in Table 1. In the Table they are classified based on their capacity to achieve CN6 (**3**, **9**, **11, 12, 13**)[93,97,98,99] or CN7 (**2, 8, 10, 14**)[100] at high oxidation states and also on the number of anionic charges (***n***$^{-}$) provided by the ancillary ligands. Further, the redox potentials for the V/IV couple, both experimental and calculated, and bond dissociation energies (BDE) for the formation of H$^{\cdot}$ from Ru^{IV}-OH species are also reported.

In Figure 10 (left) are plotted the V/IV couple, $E^{o}_{(RuV=O/RuIV=O)}$ for complexes **2, 8, 10, 14,** that achieve CN7 at Ru(V), against ***n***$^{-}$, the number of anionic charges supplied by the ancillary ligands. A nice correlation can be observed where the redox potentials decrease roughly 250 mV per ***n***$^{-}$ unit. A similar trend can be observed for O_h CN6 complexes, **3**, **9**, **11, 12, 13,** with a similar slope. In addition, the two correlations are parallel but shifted cathodically by approximately 200 mV for the CN7 case with regard to that of CN6 due to the presence of one extra ligand-atom in the first coordination sphere.

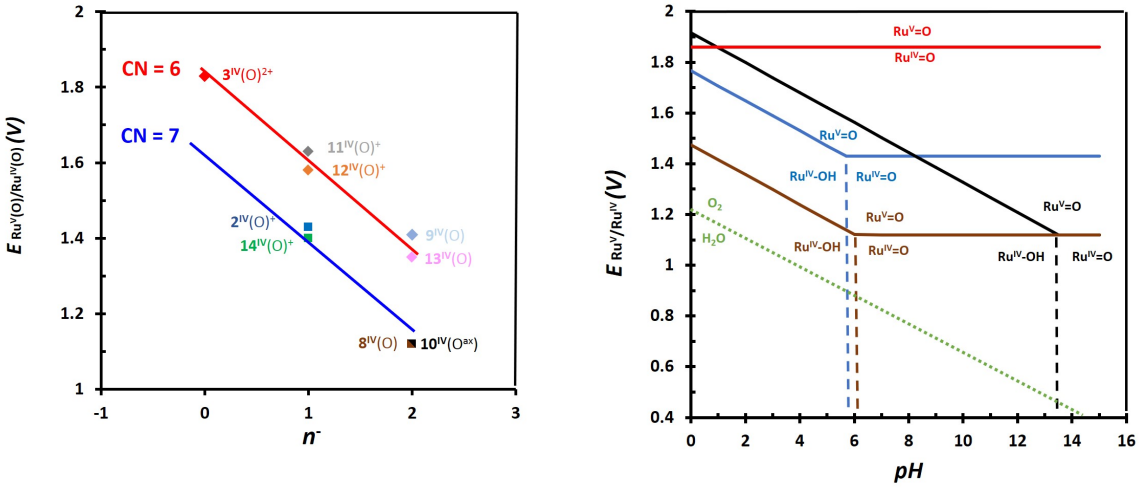

Figure 10. Left, correlation of redox potentials and number of anionic charges supplied by the bonded ligands for selected Ru-aquo complexes. Right, Pourbaix diagram for the Ru(V/IV) couple for complexes, **2** (blue line), **3** (red line), **8** (brown line), and **10** (black line).

The E^o(V/IV) *vs*. $\boldsymbol{n}^-$ correlation observed here occurs because most of the electron density removed to reach high oxidation states, is mainly removed from the Ru-O moiety. Thus, the more the anionic nature of the auxiliary ligands the higher the stabilization of high oxidation states. However, highly anionic ligands like $t5a^{3-}$ can compete with the oxidation site at high oxidation states via ligand oxidation. Indeed, theory predicts that the redox potentials for the ligand based $L^{\cdot+}Ru^{V}$=O/LRu^{V}=O couple for **9** is very similar to that of the metal based Ru-O based LRu^{V}=O/LRu^{IV}=O.[86] This illustrates the functional limit of the proposed correlation between $\boldsymbol{n}^-$ and E^o for these type of complexes as with increased $\boldsymbol{n}^-$ the ligand is becoming more prone to oxidation.

From these correlations it can be inferred that a desired Ru(V/IV) redox potential can be attained just by controlling the ancillary ligands used, the geometry around the metal center and the number of anionic charges. However, given the pH-dependency of both the Ru(V/IV) and the H_2O to O_2 redox

couples, the pK_a of the Ru(IV)-OH will be of paramount importance to evaluate the overpotential. This can be deduced from the $E^o_{(RuV=O/RuIV=O)}$ as a function of pH or Pourbaix diagram, illustrated in the right hand side of Figure 10, for complexes [**2**^{IV}(O)], [**3**^{IV}(O)]$^{2+}$, [**8**^{IV}(O)] and [**10**^{IV}(O^{ax})].

In all the cases discussed here the Ru^{V}-OH species do not exist above pH 0 because they are very acidic, their pK_a are < 0. In sharp contrast, at oxidation state IV their pK_a change significantly from values < 0 to as high as 13.5 as shown in Figure 10. This is important because for the pH values below the pK_a, a PCET process occurs with a shift of 59 mV per pH unit as is the case of the H_2O/O_2 couple. Thus, at pH values below the pK_a, the overpotential (calculated as $\eta = E^o\ (Ru^V/Ru^{IV}) - E^o\ (O_2/H_2O)$) will be constant. However, and in sharp contrast, at pH values above the pK_a, while the E^o(V/IV) remains constant the $E^o(H_2O/O_2)$ keeps decreasing by 59 mV/pH and the overpotential increases accordingly. Two extreme cases shown in Figure 10 show this point. For complex [**3**^{IV}(OH)]$^{3+}$ the pK_a < 0 (pK_a^{calc} = -8.9) and thus the predominant species is the [**3**^{IV}(O)]$^{2+}$ over the whole 0-14 pH-range. Thus, the couple does not depend on pH (as can be seen in Figure 10, right, red line) and in this case only an electron transfer process takes place. Consequently, at pH = 0 the overpotential is 0.63 V but at pH = 14 increases up to 1.46 V. On the other hand, for complex [**10**^{IV}(OH^{ax})]$^{+}$ the pK_a is 13.5 (pK_a^{calc} = 11.8) and for this complex the predominant species over the pH range 0-13.5 is the Ru^{IV}-OH (see Figure 10, right, black line). As a consequence of this, the overpotential remains constant over this pH zone with a value of 0.68 V. The Pourbaix diagram in Figure 10 (right) also reflects the strong effect of the number of anionic moieties coordinated to the metal center (***n***$^{-}$) in CN7 complexes that have the same pK_a, that is comparing complex [**8**^{IV}(OH)]$^{+}$ and [**2**^{IV}(OH)]$^{+}$, as can be observed in Figure 10 brown and blue lines respectively. Their oxidation potentials are virtually parallel to one another over the whole pH range and as a consequence the overpotential is approximately 300 mV lower for [**8**^{IV}(OH)]$^{+}$ than for [**2**^{IV}(OH)]$^{+}$.

Increasing the coordination number and the number of anionic groups coordinated as auxiliary ligands, in general reduces the potentials for the V/IV redox couple. However, a large increase on the electron density delivered at the metal center not only reduces the redox potential but also dramatically decreases the acidity of Ru^{IV}-OH species and thus increases its pK_a value. The interplay between redox potential and pK_a can be perceived by comparing E^o and pK_a for complexes $[\mathbf{3}^{IV}(O)]^{2+}$ and $[\mathbf{10}^{IV}(OH^{ax})]^{+}$, which constitutes a paradigmatic example in his respect. At pH 13.5 for the dianionic and CN7 complex $[\mathbf{10}^{IV}(OH^{ax})]^{+}$, the $E^o_{V/IV}$ = 1.12 V that is 730 mV lower than that of $[\mathbf{3}^{IV}(O)]^{2+}$ ($E^o_{V/IV}$ = 1.85 V), which is CN6 and contains only neutral auxiliary ligands. However at pH = 0 the $E^o_{V/IV}$ of $[\mathbf{10}^{IV}(OH^{ax})]^{+}$ is 1.91 V and is actually 80 mV higher than that of $[\mathbf{3}^{IV}(O)]^{2+}$, that is pH independent. Thus at pH = 0 the presence of strong donating groups is not translated into a reduction of the redox potential. This counterintuitive effect is mainly due to the different pH-dependency of the $E^o_{V/IV}$ couple that in turn is governed by the pK_a of the Ru(IV)-OH group. Indeed, for the CN6 complex $[\mathbf{3}^{IV}(OH)]^{3+}$ that has ligands with no charge, theoretical calculations predict a $pK_a^{calc} = -8.9$, but for the seven coordinated $[\mathbf{10}^{IV}(OH^{ax})]^{+}$, that contains two anionic charges with a hydroxido ligand situated axially, the pK_a remarkably increases up to 13.5 (pK_a^{calc} = 11.8), an increase in acidity of more than 19 orders of magnitude.

Another interesting comparison is also that of the pK_a of complexes $[\mathbf{8}^{IV}(OH)]^{+}$ (pK_a = 6.0) and $[\mathbf{10}^{IV}(OH)^{ax}]^{+}$ (pK_a = 13.5) that have the same Ru(V/IV) potentials at pH 13.5, because they are pseudo-isomers (they have the same type of auxiliary ligands namely, 4 pyridyl and 2 carboxylato, although organized in a different manner) but have completely different pK_a values (see Figure 10, right, black and brown lines respectively). As a consequence of this at pH 13.5 they possess identical overpotentials of 720 mV but at pH 6 the overpotential of $[\mathbf{8}^{IV}(OH)]^{+}$ decreases by 390 mV with regard to that of $[\mathbf{10}^{IV}(OH^{ax})]^{+}$ that remains constant along the whole pH-range.

The 7.5 orders of magnitude increase in the acidity of $[\mathbf{8}^{IV}(OH)]^{+}$ compared to $[\mathbf{10}^{IV}(OH)^{ax}]^{+}$ with nearly the same ligands, is attributed to a second coordination sphere effect. In particular, to the different effects of hydrogen bonding interactions via solvated water molecules at the Ru^{IV} species that occur in the equatorial or axial positions respectively as depicted in Figure 11. Complex $[\mathbf{8}^{IV}(OH)]^{+}$, with two anionic charges and coordination seven has significant intramolecular H-bonding at the equatorial zone between the Ru-OH moiety and the adjacent Ru-carboxylato group thanks to the 72° angles of the D_{5h} geometry. As a consequence $[\mathbf{8}^{IV}(OH)]^{+}$ has a pK_a = 6.0 via decoordination of one of the carboxylate groups as suggested by DFT calculations. Thus a better description of this acid-based process involves the solvated acid-base pair,

$$\{[Ru^{IV}(OH)(bda\text{-}\kappa\text{-}N^2O^2)(py)_2](H_2O)\}^{+} \rightarrow \{[Ru^{IV}(O)(bda\text{-}\kappa\text{-}N^2O)(py)_2](H_2O)\} + H^{+} \quad pK_a = 6.0 \qquad (5)$$

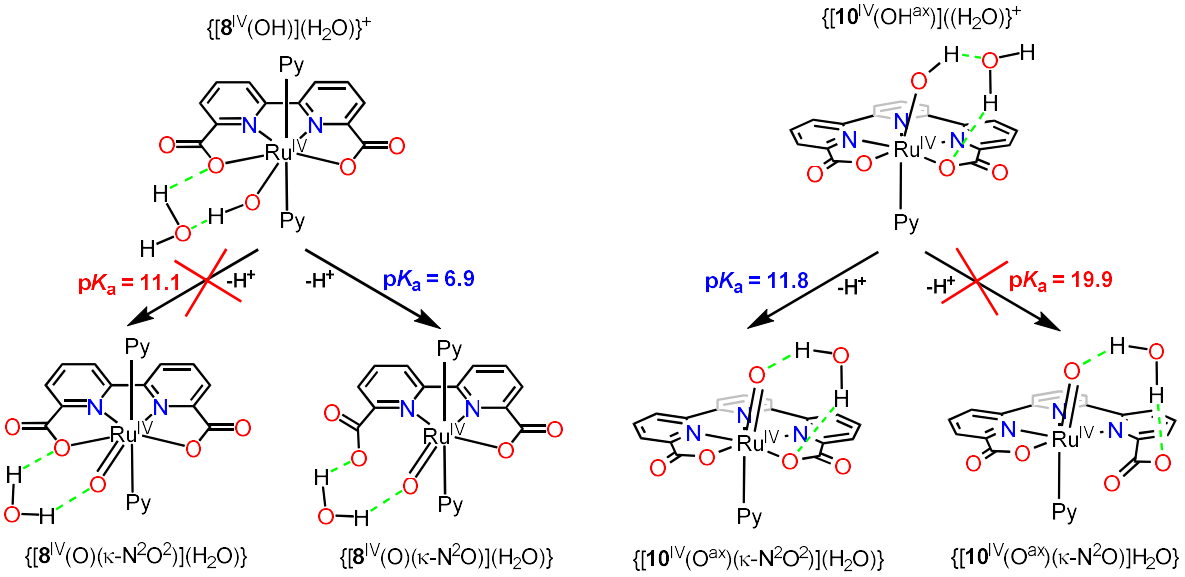

Figure 11. Solvated acid base pairs for hydroxido complexes $\mathbf{8}^{IV}$ and $\mathbf{10}^{IV}$. pK_a are calculated values based on DFT.

This is in contrast with [**10**^{IV}(OH^{ax})]$^{+}$ its pseudo-isomer, that has a pK_a = 13.5, where such an interaction is not favorable because the Ru^{IV}=O is positioned in the axial position. This again is an example of a dramatic change in a molecular property, acidity in this case, due to ligand flexibility, hydrogen bonding and second coordination sphere effects.[35] Thus the dangling carboxylate in **2** and the decoordination of one carboxylate in **8** provide a huge increase in the Ru^{IV}-OH acidity that allows to reach low overpotentials at low pH. A similar effect is obtained for **9** thanks to the decoordination of one of the carboxylate groups.

The decoordination ability of the ligand is important since in general the increase of electron density in the Ru center will involve a decrease in the Ru(V/IV)=O redox potential but at the same time also a decrease in the acidity of the Ru(IV)-OH group. This in turn will preclude the capacity of the complex to achieve low overpotentials at low pH values.

The electronic effects exerted by the ligands to the Ru^{IV}-OH/Ru^{V}=O couple quantified based on pK_a and E^o are also interesting from the point of view of their homolytic O-H bond dissociation energies (BDE). The Ru^{IV}-O-H BDE have been calculated using the Bordwell equation[101] and are presented in Table 1. These values are also of interest for the design of redox catalysts for organic transformations.[102] For the Ru(IV/III) couple the BDE range within the 80-90 kcal/mol as is also the case with Fe(III/II) couple[103] and related Mn(IV/III) complexes.[104,105,106] These values limit the potential range of substrate oxidation to substrates such as, phenol, toluene, xanthene and 1,4-cyclohexadiene among others, that are relatively easy to oxidize. However, for the most interesting organic substrates like benzene or saturated alkanes such as methane, these catalysts do not have a sufficiently high thermodynamic driving force. For the complexes described in Table 1, whose oxidative power is based on the Ru(V/IV) couple, the BDE energies are much higher within the range of 100-118 kcal/mol enabling a larger scope of organic substrates including

saturated alkanes. For instance, complex [**10**^{V}(O^{ax})]$^{+}$ can potentially oxidize benzene and methane as indicated in the equations 6-7 below.[107]

Ru^{V}=O + Me-H -> Ru^{IV}-O-H + $Me^{\bullet}$ $\Delta H^{o} = -13.0$ kcal/mol (6)

Ru^{V}=O + Ph-H -> Ru^{IV}-O-H + $Ph^{\bullet}$ $\Delta H^{o} = -6.7$ kcal/mol (7)

The key to such a high driving force is not only the access to the Ru(V) high oxidation state but also to a low pK_a value that is achieved based on H-bonding as described earlier.

6. Ligand Influence on Kinetics and Mechanism: Second Coordination Sphere Effects.

The ideal water oxidation catalyst should work desirably at the lowest overpotential and with the highest rate possible. In the previous sections we have dealt with how the potentials of the redox couples can be influenced using ancillary ligands. In this section we will discuss the capacity of these ancillary ligands to alter the kinetics of the water oxidation catalysis.

Figure 12 shows the catalytic cycle proposed for the Ru-tda complex **2**^{II} that follows a WNA mechanism. The initial CN6 complex Ru(II)-OH_2 at pH < 7, undergoes first a one electron transfer followed by a couple of PCET processes to reach Ru(V)=O. The latter is associated with a large electrocatalytic wave. Once Ru(V) is generated it reacts with a solvent water to form Ru(III)-OOH intermediate as indicated by DFT calculations, that is further oxidized by PCET to Ru(IV)-OO. Finally release of dioxygen regenerates the initial Ru(II) complex completing the catalytic cycle, as depicted in Figure 12.

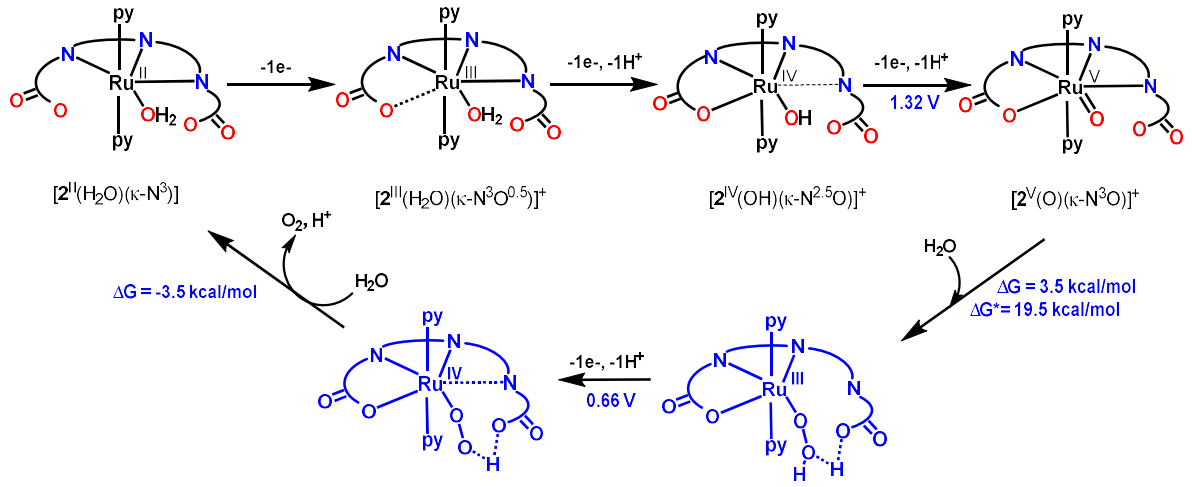

Figure 12. Water oxidation catalytic cycle proposed for **2**. The arc containing three N and four O represent the tda^{2-} ligand. Oxidation potentials and free energies are calculated values based on DFT.

For this particular complex, theory predicts the O-O bond formation (Figure 13) as the rate-determining step (RDS), which is in agreement with the observed first order kinetics with regard to [Ru].[37,108]

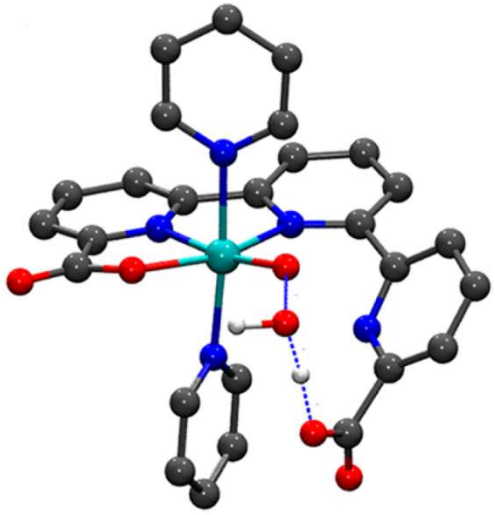

Figure 13. DFT calculated transition state structure for the reaction of $[\mathbf{2}^{V}(O)]^{+}$ with H_2O to give $[\mathbf{2}^{III}(OOH)] + H^{+}$. The solid blue line shows the formation of the O-O bond while the dashed blue line represents the intramolecular H^{+} transfer from the incoming solvent water molecule.

The kinetic performance of selected water oxidation catalysts is gathered in Table 1. Both chemical and electrochemical techniques are used to calculate catalytic rate constants. Electrochemically, the FOWA methodology [39,109] constitutes an easy and convenient tool to extract kinetic data, as depicted in Figure 14 where a catalytic Tafel plot is shown for a few complexes.

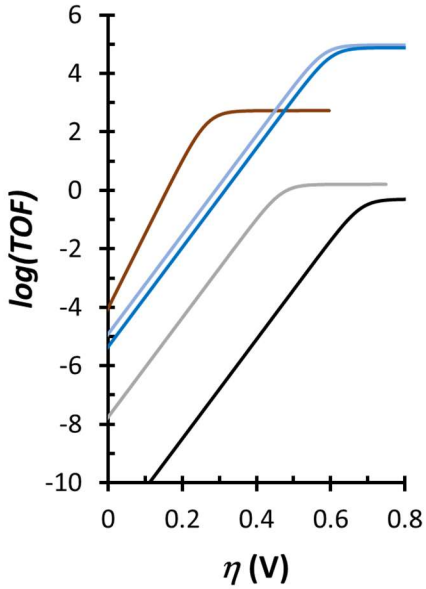

Figure 14. Catalytic Tafel plots for complexes **2** (dark blue), **8** (brown), **9** (light blue), **10** (black) and **11** (gray). The kinetic data of complexes **2**, **8**, **9** and **10** correspond to pH = 7 whereas for complex **11** is at pH = 1. Complexes **2**, **9** and **10** oxidize water following a first order mechanism in respect to the concentration and therefore their plots are concentration independent. In the case of complex **8**, its mechanism is second order in respect to the concentration and therefore its Catalytic Tafel Plot is concentration dependent. A concentration of 10 mM is used for the Catalytic Tafel Plots of **8**.

It is interesting to compare here the kinetic performance of complex $[\mathbf{2}^{IV}(OH)]^{+}$, and $[\mathbf{10}^{IV}(OH^{ax})]^{+}$ both containing the tda^{2-} ligand but with the Ru-hydroxido group located in the equatorial or axial positions respectively. At pH = 7 the Ru(V/IV) redox couples appear at 1.43 V for **2** and 1.49 V for

10 and thus they represent overpotentials of 610 and 680 mV respectively. However, even though **10** has a 60 mV higher thermodynamic driving force than **2**, the latter is more than 4 orders of magnitude faster (TOF_{max}: 0.4 s^{-1} for **10** and 7,700 s^{-1} for **2**). This enormous increase in the water oxidation kinetics is associated with the capacity of the dangling carboxylate in **2** that acts as an intramolecular base thus accepting a proton at the O-O bond formation step from the incoming water molecule (equation 8).

$$[\mathbf{2}^{V}(O)]^{+} + H_2O \rightarrow [\mathbf{2}^{III}(OOH)] + H^{+} \quad (8)$$

The consequence of this is a drastic reduction the free energy of activation (see the TS in Figure 13 and Tafel plot in Figure 14). This kinetic effect is conceptually similar to the rate enhancement that most catalysts undergo when an external base is added in solution. However in this case the proton transfer that occurs intermolecularly increases the rate by 3-3 fold (less than an order of magnitude).[110] The increase of the kinetics associated to the intramolecular proton transfer is reminiscent to other proton transferring bifunctional systems, such as the Ni complexes reported by Dubois laboratory for hydrogen evolution[22] or the control of alkene isomerization through intramolecular H transfer.[111]

Likewise, at pH 7 it is also interesting to observe that $[\mathbf{3}^{IV}(O)]^{2+}$ has a TOF of 0.05 s^{-1} an overpotential of 1.04 V (measured at pH = 1.0).[93] This is in contrast to $[\mathbf{2}^{IV}(OH)]^{+}$ that has a TOF_{max} of 7,700 s^{-1} even with a lower η of 610 mV, that is more than 5 orders of magnitude faster than that of $[\mathbf{3}^{IV}(O)]^{2+}$. This phenomenon is again a consequence of the absence of a pendant base in the latter that can generate an intramolecular hydrogen bonding.

It is also of interest to note here that the Ru complex [**9**^{IV}(O)]$^{-}$ with the trianionic ligand t5a^{3-} generates a six coordinated Ru(V) active species that also contains a pendant arm capable of acting as an intramolecular base at the transition state (Figure 8, right). For [**9**^{IV}(O)]$^{-}$ the overpotential is 670 mV and it oxidizes water to dioxygen at 9,400 s^{-1}, which is a bit faster than that of **2.** In this case with comparable intramolecular base effect the kinetics seems to be driven by the thermodynamics.

Finally, at pH 7, [**8**^{IV}(O)] has lowest overpotential of all complexes discussed here with a value of 300 mV. Under these conditions at [Ru]= 10 mM, [**8**^{IV}(O)] reaches a TOF_{max} of 25 s^{-1} as can be observed in the Tafel plot shown in Figure 14. For concentrations of [**8**^{IV}(O)] < μM, it would not possible to establish a direct comparison since it follows an I2M mechanism via a dimerization of the seven coordinated active species and the O-O bond formation is the rate determining step. It is enlightening to see that when the py axial ligands in [**8**^{V}(O)]$^{+}$ are exchanged by 6-methoxyisoquinoline (MeO-isoq), the catalytic rate of the catalyst [Ru^{II}(bda)(MeO-isoq)$_2$], increases by more than two orders of magnitude with regard to that of [**8**^{V}(O)]$^{+}$. This spectacular increase in rate is due to the π-π interaction between the axial ligands favoring the dimerization process that generates the O-O bond formation reaction. Thus the extended π -system decreases the free energy of activation by favoring the approach between the two monomers that end up making the O-O bond, as proposed based on DFT calculations.[36,112]

The O-O bond formation for Ru complexes occurs typically at formal oxidation state V. At this oxidation state an important degree of electron density is removed also from the oxygen atom and as a consequence, the latter has an important degree of radical character. Thus a simple description of the Ru-O bonding involves the resonance forms: Ru(V)=O <-> Ru(IV)-O$^{\cdot}$. The computed spin densities for the ground state doublet structures of formally Ru(V)=O species indicate very similar unpaired spin densities for a series of complexes investigated with approximately 0.5 net α spin on both Ru and O atoms. Figure 15 shows plotted unpaired spin

densities for representative examples, $[\mathbf{2}^{V}(O)]^{+}$, $[\mathbf{10}^{V}(O^{ax})]^{+}$ that follow a WNA mechanism and $[\mathbf{8}^{V}(O)]^{+}$ that dimerizes via an I2M mechanism. This distribution of spin densities implies that the electron removal at high oxidation states is shared mainly by the Ru and the O atoms of the Ru-O group, which in turn explains why remote electronic perturbations are not effective to influence high oxidation state redox potentials neither TOFs.

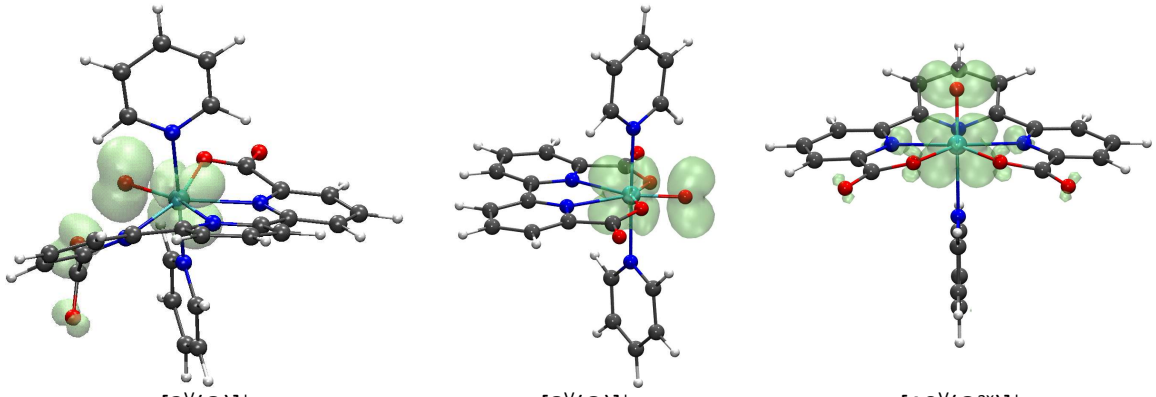

$[\mathbf{2}^{V}(O)]^{+}$
ρ_α (Ru) = 0.4
ρ_α (O) = 0.5

$[\mathbf{8}^{V}(O)]^{+}$
ρ_α (Ru) = 0.5
ρ_α (O) = 0.5

$[\mathbf{10}^{V}(O^{ax})]^{+}$
ρ_α (Ru) = 0.6
ρ_α (O) = 0.3

Figure 15. Unpaired spin density plots (isovalue = 0.002) for $[\mathbf{2}^{V}(O)]^{+}$, $[\mathbf{8}^{V}(O)]^{+}$ and $[\mathbf{10}^{V}(O^{ax})]^{+}$ where net α spin density (ρ_α) is shown in green. Color code used: Ru, cyan; N, blue; O, red; C, gray; and H, white.

The similarity in the computed spin densities indicates that the electronic nature of the Ru^{V}=O group is not responsible for accessing the WNA or I2M mechanism. It thus points out that second coordination sphere effects, such hydrogen bonding, accessible pendant bases, or supramolecular π-π interactions, solvent and steric effects are the main factors that drive the catalyst towards the WNA or I2M mechanisms. Further the WNA mechanism can also benefit from a Grotthuss type of

mechanism where the hydrogen bonded water molecules act as a base and proton relay.[113,114,115116,117]

Further, in analogues of $[Ru^{IV}(OH)(bda\text{-}\kappa\text{-}N^2O^2)(Me\text{-}py)_2]^+$, $[\mathbf{8}^{IV}(OH)]^+$, containing phosphonate groups $[Ru^{IV}(OH)(Hbpc\text{-}\kappa\text{-}N^2O^2)(Me\text{-}py)_2]^+$ and $[Ru^{IV}(OH)(H_2bpa\text{-}\kappa\text{-}N^2O^2)(Me\text{-}py)_2]^+$, the phosphonate group can act as an intramolecular proton source upon electron transfer giving rise to an intramolecular proton coupled electron transfer (i-PCET) that facilitates accessing high oxidation states at low potentials. In addition, these complexes follow a WNA mechanism and at the O-O bond formation step, the phosphonate group is proposed to act as an intramolecular proton acceptor, thus reducing free energy of activation.[90]

Some additional examples that elegantly illustrate the mechanistic flexibility are the macrocyclic trimeric Ru-bda complex $[(Ru^{II}(bda))_3(\mu\text{-}1,4\text{-}pbp)_3]$, **15**,[118,119,120] where the 1,4-bpb ligands act in a bridging manner (see Chart I and Figure 16) and the encapsulation of the Ru-bda complex in a nanosphere.[121]

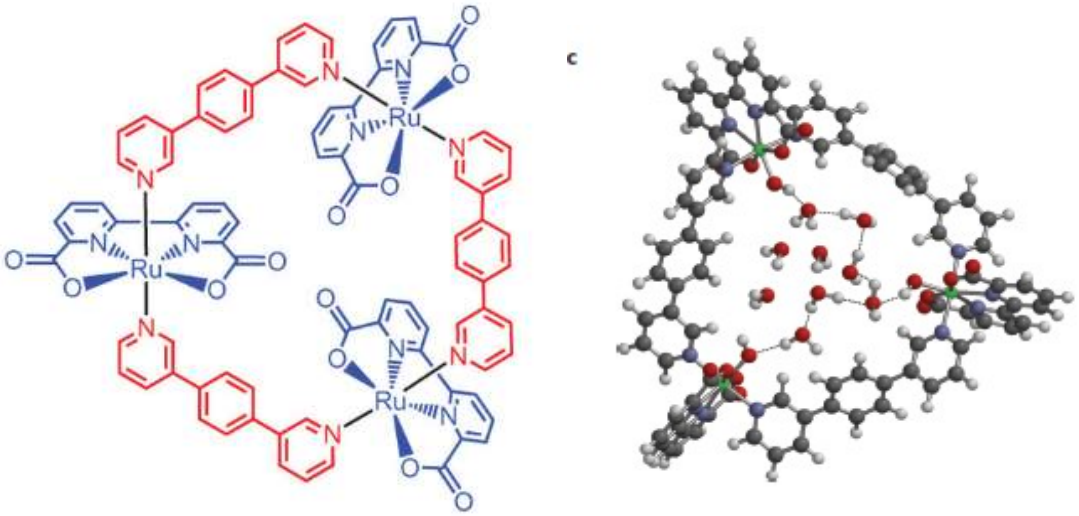

Figure 16. Left, drawing of complex $[(Ru^{II}(bda))_3(\mu\text{-}1,4\text{-}bpb)_3]$, **15**. Right, DFT calculated structure for $[\mathbf{15}^{IV}(OH)]^{3+}$, showing the intricate hydrogen bonding network of solvent water molecules

inside the cavity and associated with the three Ru-OH groups. Color code: Ru, green; N, blue; O, red; C, black; H, white. Reprinted with permission from Reference [118].

In **15**, the trimeric complex, creates a cavity that traps a large number of hydrogen bonded water molecules inside that in turn are strongly hydrogen bonded to the three Ru-OH active sites. As a consequence of this the Ru-OH groups are directed towards the inner part of the cavity, thus clearly disfavoring the dimerization process and thus following the WNA mechanism in contrast to the behavior of its mononuclear homologue, $[\mathbf{8}^{V}(O)]^{+}$, that reacts via an I2M mechanism. In the second example, a Ru-bda derivative containing a 3-pyridysulphonate as axial ligands (3-SO_3-py^-), $[Ru^{II}(bda\text{-}\kappa\text{-}N^2O^2)(3\text{-}SO_3\text{-}py)_2]^{2-}$, is isolated within the cavity of a nanosphere containing endohedral guanidinium site (See Figure 17).

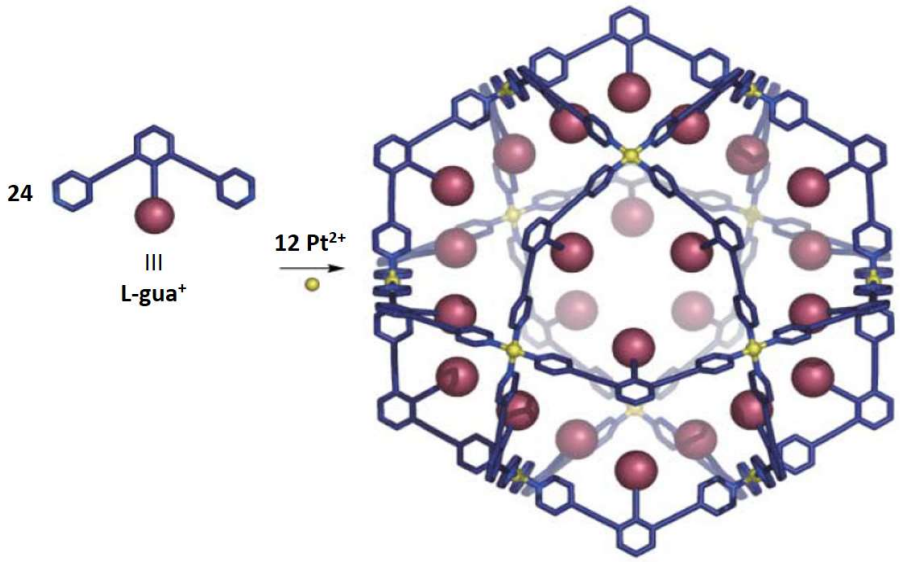

Figure 17. Self-assembly of endoguanidium $[Pt_{12}(L\text{-}gua)_{24}]^{48+}$ molecular spheres from a Pt(II) precursor and the bidentate ligand L-gua^+. The red ball represents the guanidium group of the L-

gua$^+$ ligand where the [Ru^{II}(bda-κ-N^2O^2)(3-SO_3-py)$_2$]$^{2-}$ catalyst precursor can interact via hydrogen bonding. Adapted from reference 122 and reprinted with permission.

The nanosphere is made out of 12 units of Pt(II) and 24 units of L-gua$^+$, that self-assemble in solution[122] forming a capsule of formula, [Pt_{12}(L-gua)$_{24}$]$^{48+}$ leaving an internal cavity with an approximate diameter of 4.3-4.9 nm. In the presence of a solution of [Ru^{II}(bda-κ-N^2O^2)(3-SO_3-py)$_2$]$^{2-}$, the self-assembling process traps a few molecules of the catalyst precursor within the cavity of the nanosphere thanks to the hydrogen bonding interaction between the guanidium residues and the sulfonate groups of the catalyst precursor. It is found that under catalytic conditions at low local [Ru] the rds is the bimolecular interaction and thus it follows an I2M mechanism, while at high local [Ru] the preceding step, the oxidation of Ru(IV)-OH to formally Ru(V)=O, is the rds similarly to what had been previously proposed in homogeneous phase.[35,112] Finally, the Ru-bda complex has been anchored onto solid supports following different strategies.[123,124,125,126,127] Under constrained mobility the I2M mechanism can't operate and thus the Ru-bda catalysts need to operate via the WNA high energy pathway slowing down kinetics. This allows to characterize a Ru(V)=O intermediate[123] but at the same time enables deactivation pathways to occur leading to the degradation of the molecular complex towards RuO_2, that ends up being the only active water oxidation catalyst after a few turnovers.[124] Several Ru-bda type of complexes have been reported in the literature anchored on different supports claiming they act molecularly.[125-127] However, the fate of the catalyst has never been checked after or during catalysis turnover and thus the really active catalyst is not known and even under these conditions it could be just RuO_2.

7. Conclusions.

The multiple roles of the ligands in seven coordinated Ru water oxidation catalysts have been uncovered through a detailed and careful exploration of the underlying coordination chemistry. This has been achieved via a thorough analysis of the electrochemical, spectroscopic and kinetic properties of reaction intermediates involved in the catalytic cycles complemented with computational studies, which altogether provide a very complete description of the systems.

In seven coordinated Ru complexes the flexible/adaptative multidentate equatorial auxiliary ligands (L_{fame}) play a fundamental role in the overall performance of the catalyst. Thus the design of the pentadentate L_{fame} ligands must take into account the need to adapt to the coordination demands of the Ru metal center at different oxidation sates both from a geometrical and from an electronic perspective. From a geometrical perspective this involves the rearrangement of the first coordination sphere of the Ru complexes since at oxidation state II and III they will be six coordinated with pseudo-octahedral geometry whereas at oxidation state IV and V they will have the option to become seven coordinated with a pentagonal bipyramidal type of geometry. From an electronic perspective the pentagonal bipyramidal geometry will bring additional accessibility to high oxidation states by the coordination of one more Lewis base donor.

The mismatch in ligand coordination capacity by L_{fame} with regard to the metal coordination number desired by the metal center at the different oxidation states, generates the interesting phenomena of fractional coordination, dynamic behavior due to the dangling carboxylate and the multiple equilibria observed including also the competition with exogenous monodentate ligands for a position at the first coordination sphere of the metal center.

The L_{fame} ligands can strongly influence the thermodynamics of the corresponding Ru-aquo complexes namely E^o and pK_a, based on their electronic donation capacity. Indeed, a good correlation exists for these Ru-aquo complexes between the E^o(V/IV) values and the sum of

anionic groups bonded to the metal center. This is nicely observed for both six and seven coordinated Ru complexes (see Figure 10). The electronic perturbation exerted by the ligands is also strikingly put forward by the large differences in the acidity of the Ru^{IV}-OH group that depending on the ligand framework can differ in more than 19 orders of magnitude. The L_{fame} ligands are also responsible for drastically decreasing pK_a values by transitorily decoordinating from the metal center, providing a route for achieving low overpotentials for water oxidation at low pH values. Finally, the combination of redox potentials and pK_as determines the energy needed for the homolytic bond scission on the Ru^{IV}O-H group that ranges from 100 to 110 Kcals/mol, thus making them thermodynamically competent for the oxidations of a vast array of organic substrates including benzene and methane.

The L_{fame} ligands also affect the kinetics of the water oxidation catalysis especially through second coordination sphere effects. For complexes where the O-O bond formation is the rate determining step and operating mechanism is WNA, the intramolecular proton transfer is the key phenomenon that drastically reduces the activation free energies. This is elegantly and irrefutably demonstrated by the Ru-tda complexes with and without access to the dangling carboxylate and by the Ru-t5a case. For the complexes following an I2M mechanism supramolecular π-π stacking interactions via the axial ligands can also provide a very low energy pathway as is the case of [Ru^{II}(bda)(MeO-isoq)$_2$].

Second coordination sphere effects are also responsible for selecting the O-O bond formation pathway, either WNA or I2M, since the electronic structure of the Ru^{V}=O active intermediate is very similar in all the cases studied as asserted by computational analysis.

The combination of all the factors underlined above show that the combination of L_{fame} ligands and the Ru metal center provides an excellent platform for the design of extremely powerful and robust water oxidation catalysts.

There are still several challenges in the molecular water oxidation catalysis field that lie ahead. The best catalysts turn within the microsecond time scale but ideally it would be nice to get even faster catalysts that turn at the nano-second time scale or even faster. This will be extremely useful because it can improve the efficiency of light induced photoanodes in water splitting devices. In light induced water oxidation, the water oxidation reaction is typically the slow step.[128] Thus, fast molecular water oxidation catalyst can improve the stability of the photoanode by reducing the lifetime of the oxidized anode material. A second important challenge is the transferring of all the knowledge and concepts obtained from the Ru complexes described here to earth abundant first row transition metal complexes, especially to iron. While there is no reason why this should not be possible, it is obvious that that chemistry related to first row transition metals is substantially different from that of Ru, especially from ligand substitution kinetics perspective. Thus special care should be taken for the development of molecular first row transition metals otherwise the real catalysts might end up being just the corresponding oxide; a chemistry already developed some time ago.[129,130,131]

Another important challenge is the construction of an efficient visible light induced water splitting device that contains a fast molecular water oxidation catalyst. For this purpose, the molecular catalyst needs to be attached to a solid electrode or a semiconductor with large surface areas, where a large catalyst coverage is achieved, so that high current densities can be accomplished.

8. Acknowledgments.

Sustained support from MINECO, FEDER and AGAUR are gratefully acknowledged. Recent grants include CTQ2015-64261-R, CTQ2016-80058-R, CTQ2015-73028-EXP, SEV 2013-0319, ENE2016-82025-REDT, CTQ2016-81923-REDC, and 2017-SGR-1631. The work at Brookhaven National Laboratory (M.Z.E.) was carried out under contract DE-SC0012704 with the U.S. Department of Energy, Office of Science, Office of Basic Energy Sciences, and utilized computational resources at the BNL Center for Functional Nanomaterials (CFN). The CFN is a U.S. DOE Office of Science Facility at Brookhaven National Laboratory, operating under contract No. DE-SC0012704.

References.

([1]) Greenwood, N. N.; Earnshaw. A. In *Chemsitry of the Elements*. Butterworth-Heinemann, 1997.

([2]) Pal, A. K.; Hanan, G. S. Design, synthesis and excited-state properties of mononuclear Ru(II) complexes of tridentate heterocyclic ligands. *Chem. Soc. Rev.* **2014**, *43*, 6184-6197.

([3]) Colasson, B.; Credi, A.; Ragazzon, G. Light-driven molecular machines based on ruthenium(II) polypyridine complexes: strategies and recent advances. *Coord. Chem. Rev.* **2016**, *325*, 125-134.

([4]) Jiang, C.-W.; Chao, H.; Hong, X.-L.; Li, H.; Mei, W.-J.; Ji, L.-N. Enantiopreferential DNA-binding of a novel dinuclear complex $[(bpy)_2Ru(bdptb)Ru(bpy)_2]^{4+}$. *Inorg. Chem. Commun.* **2003**, *6*, 773-775.

([5]) Ossipov, D.; Gohil, S.; Chattopadhyaya, J. Synthesis of the DNA–$[Ru(tpy)(dppz)(CH_3CN)]^{2+}$ conjugates and their photo cross-linking studies with the complementary DNA strand. *J. Am. Chem. Soc.* **2002**, *124*, 13416-13433.

([6]) Bruneau, C. In *Ruthenium catalysts and fine chemistry*. Springer-Verlag; Berlin, 2004.

([7]) Barry M. Trost, F. Dean Toste, and Anthony B. Pinkerton. Non-metathesis ruthenium-catalyzed C−C bond formation. *Chem. Rev.* **2001**, *101*, 2067–2096.

[8]) Arockiam, P. B.; Bruneau, C.; Dixneuf, P. H. Ruthenium(II)-catalyzed C–H bond activation and functionalization. *Chem. Rev*. **2012**, *112*, 5879–5918.

([9]) Doyle, M. P.; Duffy, R.; Ratnikov, M.; Zhou, L. Catalytic carbene insertion into C−H Bonds. *Chem. Rev.* **2010**, *110*, 704-724.

([10]) Punniyamurthy, T.; Velusamy, S.; Iqbal, J. Recent advances in transition metal catalyzed oxidation of organic substrates with molecular oxygen. *Chem. Rev.* **2005**, *105*, 2329-2364.

([11]) All the redox potentials reported in this document will be referred to NHE unless explicitly mentioned.

([12]) IPCC *Climate Change 2014: Mitigation of Climate Change* (eds Edenhofer, O. et al.) Cambridge Univ. Press, 2014.

([13]) Steffen, W.; Rockström, J.; Richardson, K.; Lenton, T. M.; Folke, C.; Liverman, D.; Summerhayes, C. P.; Barnosky, A. D.; Cornell, S. E.; Crucifix, M. et al. Trajectories of the earth system in the anthropocene. *Proc. Nat. Acad. Sci*. **2018**, *115*, 8252-8259.

([14]) Lewis, N. S. Research opportunities to advance solar energy utilization. *Science* **2016**, *351*, 353-360.

([15]) McCrory, C. C. L.; Jung, S.; Ferrer, I. M.; Chatman, S. M.; Peters, J. C.; Jaramillo, T. F. Benchmarking hydrogen evolving reaction and oxygen evolving reaction electrocatalysts for solar water splitting devices. *J. Am. Chem. Soc.* **2015**, *137*, 4347-4357.

([16]) Garrido-Barros, P.; Gimbert-Surinach, C.; Matheu, R.; Sala, X.; Llobet, A. How to make an efficient and robust molecular catalyst for water oxidation. *Chem. Soc. Rev.* **2017**, *46*, 6088-6098.

([17]) Kärkäs, M. D.; Verho, O.; Johnston, E. V.; Åkermark, B. Artificial photosynthesis: molecular systems for catalytic water oxidation. *Chem. Rev.* **2014**, *114*, 11863-12001.

([18]) Kunz, V.; Schmidt, D.; Röhr, M. I. S.; Mitrić, R.; Würthner, F. Supramolecular approaches to improve the performance of ruthenium-based water oxidation catalysts. *Adv. Energy Mater.* **2017**, *7*, 1602939.

([19]) Berardi, S.; Drouet, S.; Francas, L.; Gimbert-Surinach, C.; Guttentag, M.; Richmond, C.; Stoll, T.; Llobet, A. Molecular artificial photosynthesis. *Chem. Soc. Rev.* **2014**, *43*, 7501-7519.

([20]) McKone, J. R.; Lewis, N. S.; Gray, H. B. Will solar-driven water-splitting devices see the light of day? *Chem. Mat.* **2014**, *26*, 407-414.

([21]) Montoya, J. H.; Seitz, L. C.; Chakthranont, P.; Vojvodic, A.; Jaramillo, T. F.; Nørskov, J. K. Materials for solar fuels and chemicals. *Nat. Mater.* **2016**, *16*, 70-81.

([22]) Helm, M. L.; Stewart, M. P.; Bullock, R. M.; DuBois, M. R.; DuBois, D. L. A synthetic nickel electrocatalyst with a turnover frequency above 100,000 s^{-1} for H_2 production. *Science* **2011**, *333*, 863-866.

([23]) Costentin, C.; Drouet, S.; Robert, M.; Saveant, J. M. A local proton source enhances CO_2 electroreduction to CO by a molecular Fe catalyst. *Science* **2012**, *338*, 90-94.

([24]) Anderson, J. S.; Rittle, J.; Peters, J. C. Catalytic conversion of nitrogen to ammonia by an iron model complex. *Nature* **2013**, *501*, 84-88.

([25]) Blakemore, J. D.; Crabtree, R. H.; Brudvig, G. W. Molecular catalysts for water oxidation. *Chem. Rev.* **2015**, *115*, 12974-13005.

([26]) Singh, A.; Spiccia, L. Water oxidation catalysts based on abundant 1st row transition metals. *Coord. Chem. Rev.* **2013**, *257*, 2607-2622.

([27]) Romain, S.; Vigara, L.; A. L. Oxygen-oxygen bond formation pathways promoted by ruthenium complexes. *Acc. Chem. Res.* **2009**, *42*, 1944-1953.

([28]) Llobet, A.; Meyer, F. Water oxidation in the context of the energy challenge: tailored transition-metal catalysts for oxygen-oxygen bond formation. *Angew. Chem. Int. Ed.* **2011**, *50*, 30-33.

([29]) Lewis, N. S.; Nocera, D. G. Powering the planet: Chemical challenges in solar energy utilization. *Proc. Nat. Acad. Sci*. **2006**, *103,* 15729-15735.

([30]) Lewis, N. S.; Nocera, D. G. Correction for Lewis and Nocera, Powering the planet: Chemical challenges in solar energy utilization. *Proc. Nat. Acad. Sci*. **2007**, *104*, 20142-20142.

([31]) Gersten, S. W.; Samuels, G. J.; Meyer, T. J. Catalytic oxidation of water by an oxo-bridged ruthenium dimer. *J. Am. Chem. Soc.* **1982**, *104*, 4029-4030.

([32]) Ellis, W. C.; McDaniel, N. D.; Bernhard, S.; Collins, T. J. Fast water oxidation using iron. *J. Am. Chem. Soc.* **2010**, *32*, 163-170.

([33]) Sala, X.; Maji, S.; Bofill, R.; Garcia-Anton, J.; Escriche, L.; Llobet, A. Molecular water oxidation mechanisms followed by transition metals: State of the art. *Acc. Chem. Res.* **2014**, *47*, 504-516.

([34]) Keidel, A.; Lopez, I.; Staffa, J.; Kuhlmann, U.; Bozoglian, F.; Gimbert-Surinach, C.; Benet-Buchholz, J.; Hildebrandt, P.; Llobet, A. Electrochemical and resonance Raman spectroscopic studies of water-oxidizing ruthenium terpyridyl-bipyridyl complexes. *ChemSusChem* **2017**, *10*, 551-561.

([35]) Duan, L.; Bozoglian, F.; Mandal, S.; Stewart, B.; Privalov, T.; Llobet, A.; Sun, L. A molecular ruthenium catalyst with water-oxidation activity comparable to that of photosystem II. *Nat. Chem.* **2012**, *4*, 418-423.

([36]) Richmond, C. J.; Matheu, R.; Poater, A.; Falivene, L.; Benet-Buchholz, J.; Sala, X.; Cavallo, L.; Llobet, A. Supramolecular water oxidation with Ru–bda-based catalysts. *Chem. Eur. J.* **2014**, *20*, 17282-17286.

([37]) Matheu, R.; Ertem, M. Z.; Benet-Buchholz, J.; Coronado, E.; Batista, V. S.; Sala, X.; Llobet, A. Intramolecular proton transfer boosts water oxidation catalyzed by a Ru complex. *J. Am. Chem. Soc.* **2015**, *137*, 10786-10795.

([38]) Ru-aquo complexes can generate a family of complexes depending on their degree of protonation and oxidation state. For complexes where the properties of these different species are discussed, we will use an abbreviated nomenclature indicating so. For instance for complex $[Ru^{IV}(tda\text{-}\kappa\text{-}N^3O)(py)_2(O)^{eq}]$ we use [**2**^{IV}(O)] where the superscript indicates the formal oxidation state of the metal center and the O indicates the existence of the Ru-O group.

([39]) Matheu, R.; Neudeck, S.; Meyer, F.; Sala, X.; Llobet, A. Foot of the wave analysis for mechanistic elucidation and benchmarking applications in molecular water oxidation catalysis. *ChemSusChem* **2016**, *9*, 3361-3369.

([40]) Klauss, A.; Haumann, M.; Dau, H. Alternating electron and proton transfer steps in photosynthetic water oxidation. *Proc. Natl. Acad. Sci. U. S. A.* **2012**, *109*, 16035-16040.

([41]) Krewald, V.; Retegan, M.; Cox, N.; Messinger, J.; Lubitz, W.; DeBeer, S.; Neese, F.; Pantazis, D. A. Metal oxidation states in biological water splitting. *Chem. Sci.* **2015**, *6*, 1676-1695.

([42]) Rappaport, F.; Guergova-Kuras, M.; Nixon, P. J.; Diner, B. A.; Lavergne, J. Kinetics and pathways of charge recombination in photosystem II. *Biochemistry*, **2002**, *41*, 8518-8527.

([43]) Vogt, L.; Vinyard, D. J.; Khan, S.; Brudvig, G. W. Oxygen-evolving complex of Photosystem II: an analysis of second-shell residues and hydrogen-bonding networks. *Curr. Opin. Chem. Biol.* **2015**, *25*, 152-158.

([44]) Cox, N.; Pantazis, D. A.; Neese, F.; Lubitz, W. Biological water oxidation. *Acc. Chem. Res.* **2013**, *46*, 1588-1596.

([45]) Creus, J.; Matheu, R.; Peñafiel, I.; Moonshiram, D.; Blondeau, P.; Benet-Buchholz, J.; García-Antón, J.; Sala, X.; Godard, C.; Llobet, A. A million turnover molecular anode for catalytic water oxidation. *Angew. Chem. Int. Ed*. **2016**, *55*, 15382-15386.

([46]) *Molecular water oxidation catalysis: a key topic for new sustainable energy conversion schemes.* Llobet A. Ed.; Wiley and Sons Ltd., 2014.

([47]) Li, J.; Guttinger, R.; More, R.; Song, F.; Wan, W.; Patzke, G. R. Frontiers of water oxidation: the quest for true catalysts. *Chem. Soc. Rev.* **2017**, *46*, 6124-6147.

([48]) Sheehan, S. W.; Thomsen, J. M.; Hintermair, U.; Crabtree, R. H.; Brudvig, G. W.; Schmuttenmaer, C. A. A molecular catalyst for water oxidation that binds to metal oxide surfaces. *Nat. Commun.* **2015**, *6*, 6469-6469.

([49]) Bozoglian, F.; Romain, S.; Ertem, M. Z.; Todorova, T. K.; Sens, C.; Mola, J.; Rodríguez, M.; Romero, I.; Benet-Buchholz, J.; Fontrodona, X. et al. The Ru−Hbpp water oxidation catalyst. *J. Am. Chem. Soc.* **2009**, *131*, 15176-15187.

([50]) Concepcion, J. J.; Tsai, M. K.; Muckerman, J. T.; Meyer, T. J. Mechanism of water oxidation by single-site ruthenium complex catalysts. *J. Am. Chem. Soc.* **2010**, *132*, 1545-1557.

([51]) Shaffer, D. W.; Xie, Y.; Szalda, D. J.; Concepcion, J. J. Manipulating the rate-limiting step in water oxidation catalysis by ruthenium bipyridine–dicarboxylate complexes. *Inorg. Chem.* **2016**, *55*, 12024-12035.

([52]) Gimbert-Suriñach, C.; Moonshiram, D.; Francàs, L.; Planas, N.; Bernales, V.; Bozoglian, F.; Guda, A.; Mognon, L.; López, I.; Hoque, M. A. et al. Structural and spectroscopic characterization of reaction intermediates involved in a dinuclear Co–hbpp water oxidation catalyst. *J. Am. Chem. Soc.* **2016**, *138*, 15291-15294.

([53]) Pushkar, Y.; Moonshiram, D.; Purohit, V.; Yan, L.; Alperovich, I. Spectroscopic analysis of catalytic water oxidation by $[Ru^{II}(bpy)(tpy)H_2O]^{2+}$ suggests that $Ru^{V}{=}O$ is not a rate-limiting Intermediate. *J. Am. Chem. Soc.* **2014**, *136*, 11938-11945.

([54]) Alperovich, I.; Moonshiram, D.; Concepcion, J. J.; Pushkar, Y. Electronic structure assessment: combined density functional theory calculations and Ru $L_{2,3}$-Edge X-ray absorption near-edge spectroscopy of water oxidation catalyst. *J. Phys. Chem. C.* **2013**, *117*, 18994-19001.

([*55*]) Miessler, G. L.; Tarr, D. A. In *Inorganic Chemistry.* Pearson Prentice Hall, 2003

([56]) Kojima, T.; Hirai, Y.; Ishizuka, T.; Shiota, Y.; Yoshizawa, K.; Ikemura, K.; Ogura, T.; Fukuzumi, S. A low-spin ruthenium(IV)–oxo complex: does the spin state have an impact on the reactivity? *Angew. Chem. Int. Ed*. **2010**, *49*, 8449-8453.

([57]) Muckerman, J. T.; Kowalczyk, M.; Badiei, Y. M.; Polyansky, D. E.; Concepcion, J. J.; Zong, R.; Thummel, R. P.; Fujita, E. New water oxidation chemistry of a seven-coordinate ruthenium complex with a tetradentate polypyridyl ligand. *Inorg. Chem*. **2014**, *53*, 6904-6913.

([58]) Rapaport, I.; Helm, L.; Merbach, A. E.; Bernhard, P.; Ludi, A. High-pressure NMR kinetics. Part 34. Variable-temperature and variable-pressure NMR kinetic study of solvent exchange on hexaaquaruthenium(3+) and -(2+) and hexakis(acetonitrile)ruthenium(2+). *Inorg. Chem.* **1988**, *27*, 873-879.

([59]) Helm, L.; Merbach, A. E. Inorganic and bioinorganic solvent exchange mechanisms. *Chem. Rev.* **2005**, *105*, 1923-1960.

([60]) Moyer, B. A.; Meyer, T. J. Proton-coupled electron transfer between $[Ru(bpy)_2(py)OH_2]^{2+}$ and $[Ru(bpy)_2(py)O]^{2+}$. A solvent isotope effect (kH_2O/kD_2O) of 16.1. *J. Am. Chem. Soc.* **1978**, *100*, 3601-3603.

([61]) Weinberg, D. R. Gagliardi, C. J.; Hull, J. F.; Murphy, C. F.; Kent, C. A.; Westlake, B. C.; Paul, A.; Ess, D. H.; McCafferty, D. G.; Meyer, T. J. Proton-coupled electron transfer. *Chem. Rev.* **2012**, *112*, 4016-4093.

([62]) Gagliardi, C. J.; Vannucci, A. K.; Concepcion, J. J.; Chen, Z.; Meyer, T. J. The role of proton coupled electron transfer in water oxidation. *Energy Environ. Sci.* **2012***, 5*, 7704-7717.

([63]) Savéant, J.-M. Electrochemical approach to proton-coupled electron transfers: recent advances. *Energy Environ. Sci.* **2012***, 5*, 7718-7731.

([64]) Warren, J. J.; Tronic, T. A.; Mayer, J. M. Thermochemistry of proton-coupled electron transfer reagents and its implications. *Chem. Rev*. **2010**, *110*, 6961–7001.

([65]) Takeuchi, K. J.; Thompson, M. S.; Pipes, D. W.; Meyer, T. J. Redox and spectral properties of monooxo polypyridyl complexes of ruthenium and osmium in aqueous media. *Inorg. Chem.* **1984**, *23*, 1845-1851.

([66]) Yoshida, M.; Masaoka, S.; Abe, J.; Sakai, K. Catalysis of mononuclear aquaruthenium complexes in oxygen evolution from water: a new radical coupling path using hydroxocerium(IV) species. *Chem. Asian J.* **2010**, *5*, 2369-2378.

([67]) Maji, S.; López, I.; Bozoglian, F.; Benet-Buchholz, J.; Llobet, A. Mononuclear ruthenium–water oxidation catalysts: discerning between electronic and hydrogen-bonding effects. *Inorg. Chem.* **2013**, *52*, 3591-3593.

([68]) Ono, T.; Qu, S.; Gimbert-Suriñach, C.; Johnson, M. A.; Marell, D. J.; Benet-Buchholz, J.; Cramer, C. J.; Llobet, A. Hydrogenative carbon dioxide reduction catalyzed by mononuclear ruthenium

polypyridyl complexes: discerning between electronic and steric effects. *ACS Catal.* **2017**, *7*, 5932-5940.

([69]) Hintermair, U.; Sheehan, S. W.; Parent, A. R.; Ess, D. H.; Richens, D. T.; Vaccaro, P. H.; Brudvig, G. W.; Crabtree, R. H. Precursor transformation during molecular oxidation catalysis with organometallic iridium complexes. *J. Am. Chem. Soc.* **2013**, *135*, 10837-10851.

([70]) Wang, H. Y.; Mijangos, E.; Ott, S.; Thapper, A. Water oxidation catalyzed by a dinuclear cobalt-polypyridine complex. *Angew. Chem. Int. Ed.* **2014**, *53*, 14499-14502.

([71]) Wang, J.-W.; Sahoo, P.; Lu, T.-B. Reinvestigation of water oxidation catalyzed by a dinuclear cobalt polypyridine complex: identification of CoOx as a real heterogeneous catalyst. *ACS Catal.* **2016**, *6*, 5062-5068.

([72]) Radaram, B.; Ivie, J. A.; Singh, W. M.; Grudzien, R. M.; Reibenspies, J. H.; Webster, C. E.; Zhao, X. Water oxidation by mononuclear ruthenium complexes with tpa-based ligands. *Inorg. Chem*. **2011**, *50*, 10564–10571.

([73]) Zhou, J.; Xi, W.; Hurst, J. K. Structure and water-oxidizing capabilities of dimeric ruthenium edta complex ions. *Inorg. Chem*. **1990**, *29*, 160-167.

([74]) Harriman, A.; Pickering, I. J.; Thomas, J. M.; Christensen, P. A. Metal oxides as heterogeneous catalysts for oxygen evolution under photochemical conditions. *J. Chem. Soc., Faraday Trans. I* **1988**, *84*, 2795-2806.

([75]) Hong, D.; Mandal, S.; Yamada, Y.; Lee, Y.-M.; Nam, W.; Llobet, A.; Fukuzumi, S. Water oxidation catalysis with nonheme iron complexes under acidic and basic conditions: homogeneous or heterogeneous? *Inorg. Chem.* **2013**, *52*, 9522-9531.

([76]) Burg, A.; Wolfer, Y.; Shamir, D.; Korneweitz, H.; Albo, Y.; Maimon, E.; Meyerstein, D. The role of carbonate in electro-catalytic water oxidation by using Ni(1,4,8,11-tetraazacyclotetradecane)$^{2+}$. *Dalton Trans.* **2017**, *46*, 10774-10779.

([77]) Najafpour, M. M.; Feizi, H. Water oxidation by Ni(1,4,8,11-tetraazacyclotetradecane)$^{2+}$ in the presence of carbonate: new findings and an alternative mechanism. *Dalton Trans.* **2018**, *47*, 6519-6527.

([78]) Ullman, A. M.; Liu, Y.; Huynh, M.; Bediako, D. K.; Wang, H.; Anderson, B. L.; Powers, D. C.; Breen, J. J.; Abruña, H. D.; Nocera, D. G. Water oxidation catalysis by Co(II) impurities in $Co(III)_4O_4$ cubanes. *J. Am. Chem. Soc.* **2014**, *136*, 17681-17688.

([79]) Sens, C.; Romero, I.; Rodriguez, M.; Llobet, A.; Parella, T.; Benet-Buchholz, J. A new Ru complex capable of catalytically oxidizing water to molecular dioxygen. *J. Am. Chem. Soc.* **2004**, *126*, 7798-7799.

([80]) Maji, S.; Vigara, L.; Cottone, F.; Bozoglian, F.; Benet-Buchholz, J.; Llobet, A. Ligand geometry directs o-o bond-formation pathway in ruthenium-based water oxidation catalyst. *Angew. Chem. Int. Ed.* **2012**, *51*, 5967-5970.

([81]) Neudeck, S.; Maji, S.; Lopez, I.; Meyer, S.; Meyer, F.; Llobet, A. New powerful and oxidatively rugged dinuclear Ru water oxidation catalyst: control of mechanistic pathways by tailored ligand design. *J. Am. Chem. Soc.* **2014**, *136*, 24-27.

([82]) From now on, the mode of coordination of the tda^{2-} equatorial ligand will be crucial for the understanding of their properties. For this reason, the abbreviation where appropriate will include the denticity by which the ligand is coordinating to the metal center. For instance, for [Ru^{II}(tda-κ-N^3O)$(py)_2$] we will use, [**2**^{II}-κ-N^3O].

([83]) Matheu, R.; Ertem, M. Z.; Gimbert-Suriñach, C.; Benet-Buchholz, J.; Sala, X.; Llobet, A. Hydrogen bonding rescues overpotential in seven-coordinated Ru water oxidation catalysts. *ACS Catal.* **2017**, *7*, 6525-6532.

([84]) Matheu, R.; Benet-Buchholz, J.; Sala, X.; Llobet, A. Synthesis, structure, and redox properties of a trans-diaqua Ru complex that reaches seven-coordination at high oxidation states. *Inorg. Chem.* **2017**, *57,* 1757–1765.

([85]) Fractional coordination modes are used to indicate the presence of a long metal-ligand distance that can't be considered a bond but a contact.

([86]) Matheu, R.; Ertem, M. Z.; Pipelier, M.; Lebreton, J.; Dubreuil, D.; Benet-Buchholz, J.; Sala, X.; Tessier, A.; Llobet, A. The role of seven-coordination in Ru-catalyzed water oxidation. *ACS Catal.* **2018**, *8*, 2039-2048.

([87]) Matheu, R.; Ghaderian, A.; Francas, L.; Chernev, P.; Ertem, M.; Benet-Buchholz, J.; Batista, V.; Haumann, M.; Gimbert-Suriñach, C.; Sala, X. et al. The behavior of the Ru-bda water oxidation catalysts at low oxidation states. *Chem. Eur. J.* **2018.** *24*, 12838-12847.

([88]) Duan, L.; Fischer, A.; Xu, Y.; Sun, L. Isolated seven-coordinate Ru (IV) dimer complex with $[HOHOH]^-$ bridging ligand as an intermediate for catalytic water oxidation. *J. Am. Chem. Soc.* **2009**, *131*, 10397-10399.

([89]) Kamdar, J. M.; Marelius, D. C.; Moore, C. E.; Rheingold, A. L.; Smith, D. K.; Grotjahn, D. B. Ruthenium complexes of 2,2'-bipyridine-6,6'-diphosphonate ligands for water oxidation. *ChemCatChem* **2016**, *8*, 3045-3049.

([90]) Shaffer, D. W.; Xie, Y.; Szalda, D. J.; Concepcion, J. J. Lability and basicity of bipyridine-carboxylate-phosphonate ligand accelerate single-site water oxidation by ruthenium-based molecular catalysts. *J. Am. Chem. Soc.* **2017**, *139*, 15347-15355.

([91]) Xie, Y.; Shaffer, D. W.; Lewandowska-Andralojc, A.; Szalda, D. J.; Concepcion, J. J. Water oxidation by ruthenium complexes incorporating multifunctional bipyridyl diphosphonate ligands. *Angew. Chem. Int. Ed.* **2016**, *55*, 8067-8071.

([92]) Roeser, S.; Bozoglian, F.; Richmond, C. J.; League, A. B.; Ertem, M. Z.; Francas, L.; Miro, P.; Benet-Buchholz, J.; Cramer, C. J. et al. Water oxidation catalysis with ligand substituted Ru-bpp type complexes. *Catal. Sci. Technol.* **2016**, *6*, 5088-5101.

([93]) Wasylenko, D. J.; Ganesamoorthy, C.; Borau-Garcia, J.; Berlinguette, C. P. Electrochemical evidence for catalytic water oxidation mediated by a high-valent cobalt complex. *Chem. Commun.* **2011**, *47*, 4249–4251.

([94]) Llobet, A. Synthesis, spectral and redox properties of a new series of aqua complexes of ruthenium(II). *Inorg. Chim. Acta* **1994**, *221*, 125-131.

([95]) Duan, L.; Wang, L.; Inge, A. K.; Fischer, A.; Zou, X.; Sun, L. Insights into Ru-based molecular water oxidation catalysts: Electronic and noncovalent-interaction effects on their catalytic activities. *Inorg. Chem.* **2013**, *52*, 7844-7852.

([96]) Shaffer, D. W.; Xie, Y.; Concepcion, J. J. O–O bond formation in ruthenium-catalyzed water oxidation: single-site nucleophilic attack vs. O–O radical coupling. *Chem. Soc. Rev.* **2017**, *46*, 6170-6193.

([97]) Mognon, L.; Benet-Buchholz, J.; Llobet, A. Single site isomeric Ru wocs with an electron-withdrawing group: synthesis, electrochemical characterization, and reactivity. *Inorg. Chem.* **2015**, *54*, 11948-11957.

([98]) Tong, L.; Inge, A. K.; Duan, L.; Wang, L.; Zou, X.; Sun, L. Catalytic water oxidation by mononuclear Ru complexes with an anionic ancillary ligand. *Inorg. Chem.* **2013**, *52*, 2505-2518.

([99]) Li, F.; Li, L.; Tong, L.; Daniel, Q.; Gothelid, M.; Sun, L. Immobilization of a molecular catalyst on carbon nanotubes for highly efficient electro-catalytic water oxidation. *Chem. Commun.* **2014**, *50*, 13948-13951.

([100]) Fan, T.; Duan, L.; Huang, P.; Chen, H.; Daniel, Q.; Ahlquist, M. S. G.; Sun, L. The Ru-tpc water oxidation catalyst and beyond: water nucleophilic attack pathway versus radical coupling pathway. *ACS Catal.* **2017**, *7*, 2956-2966.

([101]) Bordwell, F. G.; Liu, W.-Z. Equilibrium acidities and homolytic bond dissociation energies of N−H and/or O−H bonds in N-phenylhydroxylamine and its derivatives. *J. Am. Chem. Soc*. **1996**, *118*, 8777-8781.

([102]) Mayer, J. A. Understanding Hydrogen Atom Transfer: From Bond Strengths to Marcus Theory. *Acc. Chem. Res*., **2011**, *44*, 36-46.

([103]) Goldsmith, C. R.; Jonas, R. T.; Stack, T. D. P. C−H bond activation by a ferric methoxide complex: modeling the rate-determining step in the mechanism of lipoxygenase. *J. Am. Chem. Soc*. **2002**, *124*, 83-96.

([104]) Caudle, M. T.; Pecoraro, V. L. Thermodynamic viability of hydrogen atom transfer from water coordinated to the oxygen-evolving complex of photosystem ii. *J. Am. Chem. Soc.* **1997**, *119*, 3415-3416.

([105]) Usharani, D.; Lacy, D. C.; Borovik, A. S.; Shaik, S. Dichotomous hydrogen atom transfer vs. proton-coupled electron transfer during activation of X–H bonds (X = C, N, O) by nonheme iron–oxo complexes of variable basicity. *J. Am. Chem. Soc.* **2013**, *135*, 17090-17104.

([106]) Hill, E. A.; Weitz, A. C.; Onderko, E.; Romero-Rivera, A.; Guo, Y.; Swart, M.; Bominaar, E. L.; Green, M. T.; Hendrich, M. P.; Lacy, D. C. et al. Reactivity of an Fe^{IV}-Oxo complex with protons and oxidants. *J. Am. Chem. Soc.* **2016**, *138*, 13143-13146.

([107]) Garrido-Barros, P.; Funes-Ardoiz, I.; Farràs, P.; Gimbert-Suriñach, C.; Maseras, F.; Llobet, A. In *Water as an oxygen source for oxidation reactions in Catalytic Oxidations in Organic Synthesis*. Muniz, K. Ed.; Georg Thieme Verlag KG, Stuttgart, 2016.

([108]) Govindarajan, N.; Tiwari, A.; Ensing, B.; Meijer, E. J. Impact of the ligand flexibility and solvent on the O–O bond formation step in a highly active ruthenium water oxidation catalyst. *Inorg. Chem.* **2018**. DOI: 10.1021/acs.inorgchem.8b00619.

([109]) Costentin, C.; Drouet, S.; Robert, M.; Savéant, J.-M. Turnover numbers, turnover frequencies, and overpotential in molecular catalysis of electrochemical reactions. Cyclic Voltammetry and Preparative-Scale Electrolysis. *J. Am. Chem. Soc.* **2012**, *134*, 11235-11242.

([110]) Song, N.; Concepcion, J. J.; Binstead, R. A.; Rudd, J. A.; Vannucci, A. K.; Dares, C. J.; Coggins, M. K.; Meyer, T. J. Base-enhanced catalytic water oxidation by a carboxylate–bipyridine Ru(II) complex. *Proc. Natl. Acad. Sci. U. S. A.* **2015**, *112*, 4935-4940.

([111]) Grotjahn, D.B.; Larsen, C.R.; Erdogan, G. Bifunctional catalyst control of alkene isomerization. *Top Catal.* **2014**, *57*, 1483-1489.

([112]) Xie, Y.; Shaffer, D. W.; Concepcion, J. J. O–O radical coupling: from detailed mechanistic understanding to enhanced water oxidation catalysis. *Inorg. Chem*. **2018**, *57*, 10533–10542.

([113]) de Grotthuss, C. J. Memoir on the decomposition of water and of the bodies that it holds in solution by means of galvanic electricity. *Biochim. Biophys. Acta* **2006**, *1757*, 871-875.

([114]) Kabbe, G.; Dre; Sebastiani, D. Proton mobility in aqueous systems: combining ab initio accuracy with millisecond timescales. *Phys. Chem. Chem. Phys.* **2017**, *19*, 28604-28609.

([115]) Vigara, L.; Ertem, M. Z.; Planas, N.; Bozoglian, F.; Leidel, N.; Dau, H.; Haumann, M.; Gagliardi, L.; Cramer, C. J.; Llobet, A. Experimental and quantum chemical characterization of the water oxidation cycle catalysed by $[Ru^{II}(damp)(bpy)(H_2O)]^{2+}$. *Chem. Sci.* **2012**, *3*, 2576-2586.

([116]) Liu, Z.; Gao, Y.; Wang, J.; Yao, Y.; Wei, Y.; Chen, X. Protonation effect on catalytic water oxidation activity of a mononuclear Ru catalyst containing a free pyridine unit. *J. Energy Chem.* **2017**, *27*, 1402–1408.

([117]) Liu, Z.; Gao, Y.; Zhang, M.; Liu, L. Design of a dinuclear ruthenium based catalyst with a rigid xanthene bridge for catalytic water oxidation. *Inorg. Chem. Commun*. **2015**, *55*, 56-59.

([118]) Schulze, M.; Kunz, V.; Frischmann, P. D.; Würthner, F. A supramolecular ruthenium macrocycle with high catalytic activity for water oxidation that mechanistically mimics photosystem II. *Nat. Chem.* **2016**, *8*, 576-583.

([119]) Kunz, V.; Schulze, M.; Schmidt, D.; Würthner, F. Trinuclear ruthenium macrocycles: toward supramolecular water oxidation catalysis in pure water. *ACS Energy Lett.* **2017**, *2*, 288-293.

([120]) Kunz, V.; Lindner, J. O.; Schulze, M.; Röhr, M. I. S.; Schmidt, D.; Mitrić, R.; Würthner, F. Cooperative water oxidation catalysis in a series of trinuclear metallosupramolecular ruthenium macrocycles. *Energy Environ. Sci.* **2017**, *10*, 2137-2153.

([121]) Yu, F.; Poole, D.; Mathew, S.; Yan, N.; Hessels, J.; Orth, N.; Ivanović-Burmazović, I.; Reek, J. N. H. Control over electrochemical water oxidation catalysis by preorganization of molecular ruthenium catalysts in self-assembled nanospheres. *Angew. Chem. Int. Ed.* **2018***, 57*, 11247–11250.

([122]) Sato, S.; Iida, J.; Suzuki, K.; Kawano, M.; Ozeki, T.; Fujita, M. Fluorous nanodroplets structurally confined in an organopalladium sphere. *Science* **2006**, *313*, 1273-1276.

([123]) Lebedev, D.; Pineda-Galvan, Y.; Tokimaru, Y.; Fedorov, A.; Kaeffer, N.; Copéret, C.; Pushkar, Y. The key Ru^{V}=O intermediate of site-isolated mononuclear water oxidation catalyst detected by in situ x-ray absorption spectroscopy. *J. Am. Chem. Soc.* **2018**, *140*, 451-458.

([124]) Matheu, R.; Francàs, L.; Chernev, P.; Ertem, M. Z.; Batista, V.; Haumann, M.; Sala, X.; Llobet, A. Behavior of the Ru-bda water oxidation catalyst covalently anchored on glassy carbon electrodes. *ACS Catal.* **2015**, *5*, 3422-3429.

([125]) Ding, X.; Gao, Y.; Zhang, L.; Yu, Z.; Liu, J.; Sun, L. visible light-driven water splitting in photoelectrochemical cells with supramolecular catalysts on photoanodes. *ACS Catal.* **2014**, *4*, 2347-2350.

([126]) Gao, Y.; Ding, X.; Liu, J.; Wang, L.; Lu, Z.; Li, L.; Sun, L. Visible light driven water splitting in a molecular device with unprecedentedly high photocurrent density. *J. Am. Chem. Soc.* **2013**, *135*, 4219-4222.

([127]) Wang, L.; Fan, K.; Chen, H.; Daniel, Q.; Philippe, B.; Rensmo, H.; Sun, L. Towards efficient and robust anodes for water splitting: Immobilization of Ru catalysts on carbon electrode and hematite by in situ polymerization. *Catal. Today* **2017**, *290*, 73-77.

([128]) Francàs, L.; Matheu, R.; Pastor, E.; Reynal, A.; Berardi, S.; Sala, X.; Llobet, A.; Durrant, J. R. Kinetic analysis of an efficient molecular light-driven water oxidation system. *ACS Catal.* **2017**, *7*, 5142-5150.

([129]) Coehn, A.; Gläser, M. Sutudien über die Bildung von Metalloxyden. 1. Über das anodische verhalten von kobalt- und nickel-lösungen. *Zeits. Anorg. Chem*. **1903**, *33,* 9-24.

([130]) Kim, T. V.; Elizarova, G. L.; Parmon, V. N. Catalytic oxidation of water to dioxygen by $Ru(bpy)^{3+}$ in the presence of mixed iron and cobalt hydroxides. *React. Kinet. Catal. Lett*. **1984**, *26*, 57-60.

([131]) Elizarova, G. L.; Matvienko, L. G.; Parmon, V. N. Oxidation of water by $Ru(bpy)^{3+}$ in the presence of Co(III) and Fe(III) colloidal hydroxides as catalysts. *J. Mol. Catal.* **1987**, *43*, 171-181.

BIOGRAPHIES

Roc Matheu obtained his bachelor degree in Chemistry from the Autonomous University of Barcelona in 2012. The same year he joined Prof. Antoni Llobet's group at the Institute of Chemical Research of Catalonia (ICIQ) where he developed his PhD in molecular water oxidation catalysis.

Mehmed Zahid Ertem received his PhD from University of Minnesota at C. J. Cramer's group. Then he was a Postdoctoral Research Associate at the Yale University with J. C. Tully and V.S. Batista, and at Brookhaven National Laboratory with J. T. Muckerman. He is currently an Assistant Chemist at Chemistry Division, Brookhaven National Laboratory.

Carolina Gimbert Suriñach completed her PhD at the Universitat Autònoma de Barcelona (UAB) in 2008. Then she performed postdoctoral research at the University of New South Wales (UNSW) and at the Institute of Chemical Research of Catalonia (ICIQ). She is currently scientific coordinator of the A. Llobet's group at ICIQ. Her research interests are focused on the (photo)catalysis field and its application in the development of an efficient and sustainable methodology for the production of environmentally friendly fuels.

Xavier Sala obtained his Ph.D. in Chemistry from the University of Girona in 2007. After postdoctoral research with P. W. N. M. van Leeuwen and A. Llobet at ICIQ, he is currently Associate Professor of Chemistry at the Autonomous University of Barcelona (UAB) where he leads the *Selective Oxidation Catalysis* (SelOxCat) research group.

Antoni Llobet received a PhD from UAB. Then he was a Postdoctoral Fellow at the University of North Carolina with T. J. Meyer and at Texas A&M University with D. T. Sawyer and A. E. Martell. He is currently a Professor of Chemistry at UAB and a Group Leader at ICIQ.

Graph. Abstract

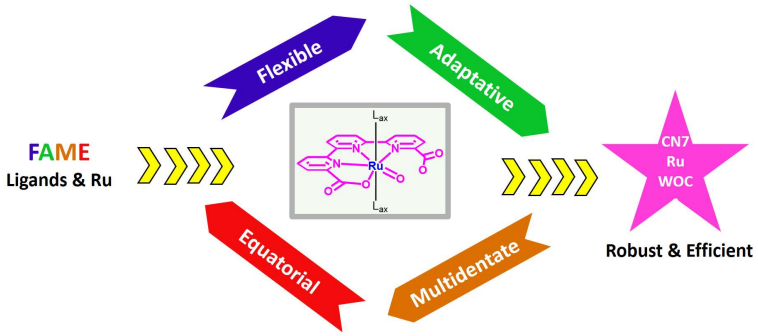

Catalysts for the water oxidation reaction are important components of energy technologies based on light induced water splitting devices. The study of molecular catalysts affords mechanistic insights that allows for the development of robust, active and energy-efficient systems. This Review describes the latest and most significant developments on Ru metal complexes that behave as powerful water oxidation catalysts and where at some stage the metal centers attain a first sphere coordination number of 7.